Living Fluids/Fluides vivants

Active suspensions and their nonlinear models

Les suspensions actives et leurs modèles non linéaires

David Saintillan [a,*], Michael J. Shelley [b]

[a] *Department of Mechanical Science and Engineering, University of Illinois at Urbana-Champaign, Urbana, IL 61801, USA*
[b] *Courant Institute of Mathematical Sciences, New York University, New York, NY 10012, USA*

A R T I C L E   I N F O

A B S T R A C T

Active suspensions, such as suspensions of self-propelled microorganisms and related synthetic microswimmers, are known to undergo complex dynamics and pattern formation as a result of hydrodynamic interactions. In this review, we summarize recent efforts to model these systems using continuum kinetic theories. We first derive a basic kinetic model for a suspension of self-propelled rodlike particles and discuss its stability and nonlinear dynamics. We then present extensions of this model to analyze the effective rheology of active suspensions in external flows, the effect of steric interactions in concentrated systems, and the dynamics of chemotactically responsive suspensions in chemical fields.

© 2013 Académie des sciences. Published by Elsevier Masson SAS. All rights reserved.

R É S U M É

Les suspensions actives, telles que les suspensions de micro-organismes auto-propulsés ou autres nageurs microscopiques artificiels, sont connues pour leur dynamique complexe et la formation de motifs en raison d'interactions hydrodynamiques. Nous résumons dans cet article les dernières avancées dans la modélisation de ces systèmes à l'aide de théories cinétiques continues. Dans un premier temps, nous développons un modèle cinétique élémentaire pour une suspension de particules auto-propulsées alongées et considérons sa stabilité et sa dynamique non linéaire. Nous présentons ensuite des extensions de ce modèle pour analyser la rhéologie effective des suspensions actives en écoulement externe, l'effet des interactions stériques dans les systèmes à forte concentration et la dynamique de suspensions chimiotactiques dans des champs chimiques.

© 2013 Académie des sciences. Published by Elsevier Masson SAS. All rights reserved.

1. Introduction

Biophysics, synthetic chemistry, colloidal physics, and materials science have all contributed in the last decade to the creation and study of *active suspensions*. These are systems in which a suspended microstructure exerts *active stresses* upon an immersing fluid, which itself provides a coupling medium through which to create large-scale dynamics. By active stresses, we mean those that arise not from the passive mechanical responses of the microstructure to thermodynamic fluctuations or to flow forcing (e.g. shearing), but rather from the conversion of energy from one form, say chemical, to another so as to

---

* Corresponding author.
  E-mail address: dstn@illinois.edu (D. Saintillan).

typically yield a change in shape. Shape change is the basic element of biological locomotion [1], and many studies of active suspensions have arisen from studying collective dynamics in biology, such as in bacterial baths or coordinated metachronal waves on ciliated organisms [2,3]. On the former, experiments on suspensions of swimming bacteria such as *Escherichia coli* or *Bacillus subtilis* have shown striking dynamics [4–7]. This includes complex flows characterized by large-scale vortices and jets with sizes and speeds much greater than those associated with swimming individuals [5,8–10]. Other observations have included the formation of spatial inhomogeneities [5,7], locally correlated motions [11,12], enhanced particle diffusion, enhanced fluid mixing and passive tracer diffusion [4,13–15].

Synthetic chemists and colloidal physicists have also become more and more adept at creating microscopic synthetic particles that can propel themselves, in some instances autonomously, such as through catalytic chemical reactions at their surfaces [16–21], or in a more directed fashion, say through interactions with externally imposed magnetic fields [22–25]. While these systems are distinct from biological ones, they may prove to provide paradigmatic examples that are not complicated by organismal sensing and behavior. Finally, not all active suspensions have microstructures that swim (at least by design). Recent experiments have also created synthetic active suspensions that are fluids filled with biological elements, such as microtubule or actin bio-polymers, motor-proteins, and fuel (ATP). There, large-scale dynamics are seen to arise instead from direct interactions between bio-polymers induced by motor-protein coupling and transport [26–28], or through interactions with substrate-bound motor-proteins [29,30].

Along with these experimental developments have been efforts by theorists to explain and predict the dynamics evinced by these systems. This has included large-scale simulation studies that seek to model the dynamics of the immersed active particles directly and to capture their interactions through the surrounding fluids. Graham and coworkers developed a "minimal" swimmer model [31], in which a particle is represented as a rigid dumbbell exerting equal and opposite localized forces on the fluid, thus creating the far-field force dipole induced by self-propulsion [32–34]. Coupling many such particles together hydrodynamically, they were able to reproduce observed features such as correlated motions at high concentrations and enhanced tracer diffusion [31,35]. Pedley and coworkers developed detailed Stokesian dynamics simulations of interacting "squirmers", propelled by a prescribed surface slip velocity, and also reported motile particle and tracer diffusion [36,37], and the development of coherent structures in their suspensions [38,39]. Recently, we also developed a detailed model in which hydrodynamically interacting rodlike particles propel themselves through a prescribed tangential stress on their surfaces [40,41]. In semi-dilute suspensions of rear-actuated particles, we observed large-scale roiling flows taking place near the system size, the enhancement of mean swimming speeds, and strong motile particle diffusion [40]. We also observed dependencies on actuation type (rear- vs front-actuated), and sharp transitions to flow instability as a function of particle concentration or system size [41].

Such particle-based models are invaluable. They yield dynamics in qualitative agreement with experiments that can be analyzed statistically and probed for scaling laws. However, because of their computational expense, they are difficult to study systematically, and because of their fundamentally discrete nature, they are difficult to plumb for analytical insights. To address this, we and others have found it very useful to study active suspensions as complex fluids, and to employ the tools of continuum mechanics, statistical physics, and coarse-graining to posit or derive continuum partial-differential-equation models [42–48]. Those models closest to first principles are often in the form of kinetic equations coupled to the equations of hydrodynamics [43,44,46]. These nonlinear systems of partial differential equations can often be reduced to yet simpler descriptions that yield insight into the dynamics, can be analyzed for stability near physically relevant steady states, or can be directly simulated to discover the nonlinear dynamics that they capture or predict.

In this exposition, we will discuss our work on nonlinear continuum modeling of active suspensions. In a first-principles approach, we begin in Section 2 with a microscopic description of a swimmer moving against a background fluid flow, perhaps created by other swimmers, and calculate how this particle moves and the stresses it creates in the surrounding fluid. Then, using a coarse-graining approach we calculate the macroscopic fluid flows that are created by many such swimmers, and this is used to derive a Smoluchowski equation for the distribution function of particle positions and orientations. This kinetic–hydrodynamic model for an active suspension is surprisingly elegant and can show a rich variety of phenomena. We discuss its analytical structure, its predictions for the development of large-scale flows and dependencies on swimmer type, and illustrate the complex dynamics that it generates. We also discuss the application of this model to study the surprising rheology of active suspensions in Section 3 and its extension to capture ordering steric interactions amongst swimmers at high volume concentration in Section 4. We then turn to our work on chemotactically responsive active suspensions in Section 5, where swimming particles modulate their dynamics in response to chemical fields that may be externally supplied (such as oxygen) or secreted and transported by the swimmers themselves.

2. Active suspension model

2.1. Smoluchowski equation and single-particle model

We outline the derivation of a kinetic theory for the hydrodynamics of a dilute suspension of motile rodlike particles [43,44]. This model closely resembles that of Doi for passive rod suspensions [49,50]. Like Doi, we evolve a distribution function $\Psi(\mathbf{x}, \mathbf{p}, t)$ of particle positions $\mathbf{x}$ and orientation vectors $\mathbf{p}$ (satisfying $\mathbf{p} \cdot \mathbf{p} = 1$) through a Smoluchowski equation that expresses conservation of particle number:

$$\partial_t \Psi + \nabla_x \cdot (\dot{\mathbf{x}} \Psi) + \nabla_p \cdot (\dot{\mathbf{p}} \Psi) = 0 \tag{1}$$
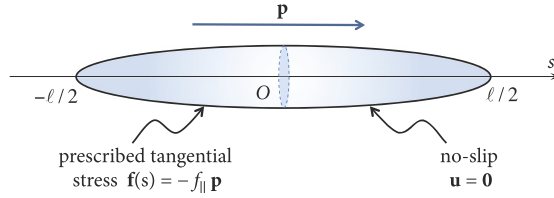
Fig. 1. A schematic of the simple rodlike swimmer model that underlies the continuum kinetic theory of Saintillan and Shelley [43,44]. The swimmer of length ℓ swims along its director $\mathbf{p}$ due to a motive stress prescribed upon its posterior surface. A no-slip condition is applied on the leading anterior half.

where $\nabla_p = (\mathbf{I} - \mathbf{pp}) \cdot (\partial/\partial\mathbf{p})$ denotes the gradient operator on the unit sphere of orientations Ω. Here $\dot{\mathbf{x}}$ and $\dot{\mathbf{p}}$ denote the conformational fluxes in space and orientation, expressions for which can be obtained by analyzing the dynamics of a single motile rod in a background flow with velocity $\mathbf{u}(\mathbf{x}, t)$.

To this end, consider a straight and slender rod of length ℓ, thickness b, and aspect ratio $r = \ell/b \gg 1$ that is suspended in a Newtonian fluid of viscosity η and moving against a background flow $\mathbf{u}(\mathbf{x}, t)$. The rod position is described by its centerline with equation $\mathbf{X}(s, t) = \mathbf{x}_c(t) + s\mathbf{p}(t)$, where $s \in [-\ell/2, \ell/2]$ is arclength, $\mathbf{x}_c$ is the rod center-of-mass (at $s = 0$), and $\mathbf{p}$ is the particle orientation vector, which also describes the direction of swimming. We assume that the rod is density-matched to the fluid and that fluid and particle inertia are both negligible. Hence, the Stokes equations govern the fluid motion, and the particle exerts zero mean force and torque on the surrounding fluid.

Local slender-body theory for the Stokes equations [51–53] relates the velocity $\partial_t\mathbf{X}(s, t)$ of a point along the rod to the force per unit length $\mathbf{f}(s, t)$ exerted by the rod on the fluid. To leading order,

$$\mu\big[\partial_t\mathbf{X}(s, t) - \mathbf{u}\big(\mathbf{X}(s, t)\big)\big] = (\mathbf{I} + \mathbf{pp}) \cdot \mathbf{f}(s, t) \tag{2}$$

where $\mu = 4\pi\eta/\ln(2r)$. As a simple model for an elongated swimmer (see Hohenegger and Shelley [54]), we consider rods upon which a constant propulsive tangential stress $-f_{\|}\mathbf{p} = -2\pi bg\mathbf{p}$, where g is the stress magnitude, is prescribed upon the posterior half ($-\ell/2 \leqslant s < 0$), whereas a no-slip condition is imposed upon the anterior half ($0 < s \leqslant \ell/2$) as depicted in Fig. 1. To accommodate the prescription of the motive stress, we must also allow a slip velocity $u_s\mathbf{p}$ along the posterior half. The model described here corresponds to a so-called *pusher particle*, such as the bacteria *Escherichia coli* and *Bacillus subtilis*, which push their cell body (the anterior) forward through the fluid through the turning of their flagellar bundle (located on the posterior end). In the case of a *puller particle*, such as the micro-alga *Chlamydomonas reinhardtii*, the situation is reversed, with the motive stress exerted on the anterior half of the rod and a no-slip condition on the posterior. A related but more sophisticated single-swimmer model was also used in the numerical simulations of Saintillan and Shelley [40,41].

As is standard in deriving continuum models (though not in particle simulations), we assume that the particle is sufficiently small that the macroscopic velocity, itself produced by boundary conditions and by the collective effect of all the other suspended swimmers, is well represented by its local linearization. Under the assumptions made above, the slender-body relation, applied to the posterior and anterior halves of the rod, respectively, yields:

$$\mu\big[\dot{\mathbf{x}}_c + u_s\mathbf{p} + s\dot{\mathbf{p}} - \mathbf{u}(\mathbf{x}_c) - s\mathbf{p} \cdot \nabla\mathbf{u}(\mathbf{x}_c)\big] = (\mathbf{I} + \mathbf{pp}) \cdot \mathbf{f}_P \tag{3}$$

$$\mu\big[\dot{\mathbf{x}}_c + s\dot{\mathbf{p}} - \mathbf{u}(\mathbf{x}_c) - s\mathbf{p} \cdot \nabla\mathbf{u}(\mathbf{x}_c)\big] = (\mathbf{I} + \mathbf{pp}) \cdot \mathbf{f}_A \tag{4}$$

The force distribution in Eq. (2) is here decomposed as $\mathbf{f}(s, t) = H_{s\in[-\ell/2,0)}\mathbf{f}_P(s, t) + H_{s\in(0,\ell/2]}\mathbf{f}_A(s, t)$ where H denotes the Heaviside function. From the condition of zero net torque, $\mathbf{f}_P$ and $\mathbf{f}_A$ must both point in the direction of $\mathbf{p}$. Applying the condition of zero total force, it is then straightforward to derive expressions for the center-of-mass and angular velocities of the rod as:

$$\dot{\mathbf{x}}_c = V_0\mathbf{p} + \mathbf{u}(\mathbf{x}_c) \tag{5}$$

$$\dot{\mathbf{p}} = (\mathbf{I} - \mathbf{pp}) \cdot \nabla\mathbf{u}(\mathbf{x}_c) \cdot \mathbf{p} \tag{6}$$

from which the force distributions $\mathbf{f}_P$ and $\mathbf{f}_A$ are then obtained as:

$$\mathbf{f}_P(s) = \left(-f_{\|} - s\frac{\mu}{2}\mathbf{pp} : \nabla\mathbf{u}(\mathbf{x}_c)\right)\mathbf{p} \tag{7}$$

$$\mathbf{f}_A(s) = \left(f_{\|} - s\frac{\mu}{2}\mathbf{pp} : \nabla\mathbf{u}(\mathbf{x}_c)\right)\mathbf{p} \tag{8}$$

Here, the single-rod translational velocity is given by $V_0 = \kappa_2\ell g/\eta$ where κ_2 is a geometric constant dependent upon the aspect ratio r [54], and more generally upon the particular shape of the motile particle. Eq. (6) is known as Jeffery's equation [55] and describes how the slender rod is rotated by the velocity gradient of the background flow. Since the rod rotates without change of length, there is also a corresponding "constraint force", proportional to $\mathbf{pp} : \nabla\mathbf{u}$, that appears in Eqs. (7)–(8) for the force distribution. In the absence of an external flow, however, we note that the force distributions $\mathbf{f}_P(s)$ and
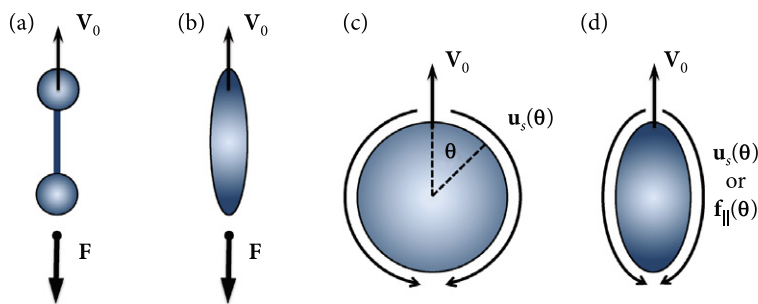
Fig. 2. Alternate models for single self-propelled particles: (a) minimal model of Graham and coworkers [31,35,58,59], in which a rigid dumbbell propels itself by exerting an off-centered force **F** on the fluid that balances the drag on the spheres; (b) rigid ellipsoid model, which generalizes the model of (a) by replacing the dumbbell by a rigid ellipsoid [60–64]; (c) classic spherical squirmer model [65–68], in which a prescribed slip velocity on the surface of a rigid sphere causes it to swim; (d) generalizations of the squirmer model to anisotropic shapes (spheroids) and more complex boundary conditions (prescribed tangential stress instead of prescribed slip) [69].

$\mathbf{f}_A(s)$ are simply given by $\pm f_\parallel \mathbf{p}$, and that the net effect of these force distributions on the fluid is therefore that of a Stokes dipole, whose sign depends on the type of swimmer (pusher vs puller). This net force dipole is a fundamental feature of neutrally buoyant microswimmers and is at the origin of the active stress that drives the large-scale dynamics in these systems.

The version of Jeffery's equation obtained from slender-body theory in Eq. (6) is strictly valid in the limit of infinite aspect ratio, and does not capture the effect of the particle thickness b on the angular dynamics; in particular, it predicts asymptotic alignment of a particle in a simple shear flow, unlike the expected Jeffery's orbits [56]. The more general and classic form of Jeffery's equation can be substituted instead to account for finite particle thickness [55]:

$$\dot{\mathbf{p}} = (\mathbf{I} - \mathbf{pp}) \cdot \left[\beta \mathbf{E}(\mathbf{x}_c) + \mathbf{W}(\mathbf{x}_c) \right] \cdot \mathbf{p} \tag{9}$$

where $\mathbf{E} = (\nabla \mathbf{u} + \nabla \mathbf{u}^T)/2$ and $\mathbf{W} = (\nabla \mathbf{u} - \nabla \mathbf{u}^T)/2$ are the rate-of-strain and vorticity tensors, respectively, and the dimensionless parameter β depends on the particle shape. For a spheroidal particle of aspect ratio r, it is obtained as $\beta = (r^2 - 1)/(r^2 + 1)$, though the validity of Eq. (9) extends to any axisymmetric particle shape [56].

From these calculations, we can now take the fluxes in the Smoluchowski equation (1) to have the form

$$\dot{\mathbf{x}} = V_0 \mathbf{p} + \mathbf{u}(\mathbf{x}) - D \nabla_x \ln \Psi \tag{10}$$

$$\dot{\mathbf{p}} = (\mathbf{I} - \mathbf{pp}) \cdot \left[\beta \mathbf{E}(\mathbf{x}) + \mathbf{W}(\mathbf{x}) \right] \cdot \mathbf{p} - d \nabla_p \ln \Psi \tag{11}$$

where the latter terms are diffusive fluxes that capture the effects of translational and rotational stochastic fluctuations, for which D and d are the corresponding diffusion coefficients. These diffusion processes can have varied origins. In the case of colloidal artificial microswimmers, they capture the effects of Brownian motion on the dynamics. In the case of biological swimmers, thermal fluctuations are typically too weak to result in significant Brownian motion, but intrinsic diffusion may still arise as a result of imperfections in the shape or swimming actuation of the particles [34,57]; in addition, particle–particle hydrodynamic interactions also result in an effective diffusion at long times [31,41].

2.2. Alternate micromechanical models

The micromechanical model described above, based on the self-propulsion of a slender particle with anisotropic drag as a result of a prescribed surface stress, is only one of many theoretical or computational swimming models that have been proposed over the years, some of which we review here.

In an early computational study of collective dynamics, Graham and coworkers [31,35,58,59] developed a minimal swimmer model that captures many of the important features of the hydrodynamics of self-propelled microorganisms. In this model, the body of a swimmer is represented as a rigid bead-rod dumbbell as illustrated in Fig. 2(a). Propulsion arises as a result of a "phantom flagellum" that exerts a force on the fluid at an off-centered point along the axis of the dumbbell. This force on the fluid results in the translation of the dumbbell at a swimming velocity of $V_0 = F/2\zeta + O(a/\ell)$, where $\zeta = 6\pi\eta a$ is the drag coefficient of each bead, a is the bead radius, and ℓ is the characteristic size of the swimmer; in this expression for V_0, hydrodynamic interactions between the two beads are neglected and would modify the velocity to order $O(a/\ell)$. Because the propulsive force exerted by the phantom flagellum is exactly balanced by the total drag force on the dumbbell, the leading effect of a swimmer on the fluid is that of a force dipole, as in the swimming rod model presented in Section 2.1. In addition, the anisotropy of the dumbbell guarantees that its orientation dynamics can also be captured by Jeffery's equation (9), so that the dumbbell model displays similar dynamics and hydrodynamic interactions as the swimming rod model. This dumbbell model was deployed in numerical simulations of confined active suspensions by Hernández-Ortiz et al. [31,35], where it was shown to capture many of the qualitative features of experiments on bacterial suspensions, including enhanced diffusivities and large-scale correlated flows. It was also used as a theoretical model by

Underhill et al. [58,59] to derive predictions for the diffusivities, correlations and stress fluctuations in dilute suspensions of swimmers.

The dumbbell model of Graham and coworkers was also generalized by others to include a spheroidal body shape, as shown in Fig. 2(b). Such a model was proposed by Haines et al. [60,61] in their study of the dilute rheology of active suspensions (see Section 3), where the authors made use of the exact analytical expressions for the mobility coefficients of a rigid spheroid [70]. This model was then later applied by the same group in numerical simulations at finite concentration to study the effect of particle hydrodynamic interactions on the dynamics and rheology of swimmer suspensions [62,63]. A similar description of self-propulsion was used in recent numerical simulations in two dimensions by Decoene et al. [64].

In an entirely different class of models, propulsion is not the result of a force exerted by a flagellum on the fluid but rather of a prescribed surface slip velocity distribution (see Fig. 2(c)), which could be a coarse-grained description of the velocity imparted on the fluid by an array of cilia distributed on the swimmer surface [71]. This so-called "squirmer" model, which was first developed by Lighthill [65] and Blake [66] and later refined by Pedley and coworkers [67,68], is appropriate to model the dynamics of ciliated microorganisms such as *Volvox* [32,72] or *Paramecium*, though it has often been used as a generic model for self-propelled particles. For an axisymmetric swimmer with zero swirl, the tangential surface slip velocity has no azimuthal component and is fully defined by a scalar function $u_s(\theta)$ of the angle θ from the leading pole of the sphere, which can take on several forms to model different types of swimmers and is best represented in terms of an expansion as:

$$u_s(\theta) = \sum_{n \geq 1} B_n \phi_n(\cos\theta) \tag{12}$$

where the orthogonal basis functions ϕ_n are defined in terms of the Legendre polynomials P_n:

$$\phi_n(\cos\theta) = \frac{2}{n(n+1)} \sin\theta \, P_n'(\cos\theta) \tag{13}$$

It can be shown that the swimming velocity of a force-free swimmer is given by $V_0 = 2B_1/3$, and that the sign of the ratio B_2/B_1 determines the type of swimmer (positive for pullers, negative for pushers). The mathematical simplicity of this model allows for an analytical solution of the fluid velocity around an isolated swimmer based on Lamb's general solution of the Stokes equations [70,73]. The model was also used in numerical simulations to study pair hydrodynamic interactions [74], as well as diffusion [37], collective motion [38,39,75], and rheology [36] in semi-dilute suspensions. The behavior of spherical squirmers in flow differs from that of rodlike swimmers owing to the shape isotropy, which corresponds to the special case of $\beta = 0$ in Jeffery's equation (9): such squirmers rotate with the flow vorticity, but there is no mechanism for them to preferentially align with the axis of extension of the strain rate tensor as in the case of rods. This seemingly small difference has profound consequences on hydrodynamic interactions between swimmers, and in fact the hydrodynamic instabilities described below in Section 2.5.2 vanish in the limit of $\beta \to 0$, as do the effects of activity on the rheology of the suspensions. Collective motion has nonetheless been reported in simulations of interacting spherical squirmers [38,39, 75], though its origins have yet to be fully elucidated and may be the result of near-field interactions or of other types of multipolar interactions not included in our basic kinetic model.

Blake's basic squirmer model has also been extended to account for shape anisotropy and more complex boundary conditions. The basic features of hydrodynamic interactions of spheroidal squirmers were recently analyzed theoretically by Spagnolie and Lauga [76], who showed a subtle dependence of hydrodynamic interactions with a rigid no-slip wall on the basic flow singularities driven by the particle, which are related to the distribution of surface slip. In a more detailed model, Kanevsky et al. [69] considered prolate spheroidal squirmers propelling themselves by prescribing the tangential stress on their surface (rather than the slip velocity), which can be thought of as a more accurate version of the basic rod model of Section 2.1. They derived an analytical solution for an isolated particle, and also performed numerical simulations using the boundary element method to study hydrodynamic interactions. A spheroidal squirmer model was also recently used to analyze locomotion in polymeric liquids [77].

It is interesting to note that all the models discussed here, with the exception of the spherical squirmer model (for which $\beta = 0$), show qualitatively similar dynamics as the rigid rod model of Section 2.1. In particular, orientational dynamics can always be captured by Jeffery's equation with an appropriate value of β depending on the exact shape of the particles [56], and the fluid flow driven by an isolated swimmer is expected to be that of a force dipole, at least sufficiently far away from the particle surface. The validity of the kinetic description of a suspension by means of the Smoluchowski equation (1) coupled to the flux equations (10)–(11) is therefore quite general as long as the swimmers are anisotropic and exert a non-zero force dipole on the fluid.

2.3. Coarse-grained active stress

To close the system of kinetic equations posed in Section 2.1, it remains to calculate how the velocity and its gradient are determined from the distribution of particle positions and orientations. This is accomplished by calculating the *extra stress* induced in the fluid by the motions of the force- and torque-free swimmers. Batchelor [78–80] provided the necessary analysis, and showed that the effective stress induced by a suspension of particles can be expressed as the volume average

of the force dipoles, or stresslets, exerted by the particles on the fluid. More precisely, given M rodlike particles suspended in a control volume of volume $\tilde{V}$, the volume-averaged extra stress produced by their motions is given by:

$$\boldsymbol{\Sigma} = -\frac{1}{\tilde{V}} \sum_{k=1}^{M} \int_{-\ell/2}^{\ell/2} \mathbf{f}_k(s) \mathbf{X}_k(s) \, \mathrm{d}s \tag{14}$$

Applied to a single rod in the absence of any background flow, this formula generates the rank-one tensorial contribution: $\boldsymbol{\Sigma}_0 = \sigma_0 \mathbf{pp}$, where the stresslet σ_0 is a measure of the force dipole exerted by a swimmer on the fluid and is expressed as $\sigma_0 = -\kappa_1 \ell^3 g$ where κ_1 is another geometric constant [54]. It is straightforward to show that the stresslet is positive for a puller, but negative for a pusher. Assuming that M is large, and passing to a distributional limit, we approximate the active stress $\boldsymbol{\Sigma}^s$ due to swimming as:

$$\boldsymbol{\Sigma}^s(\mathbf{x}, t) = \sigma_0 \int_{\Omega} \Psi(\mathbf{x}, \mathbf{p}, t)(\mathbf{pp} - \mathbf{I}/3) \, \mathrm{d}\mathbf{p} \tag{15}$$

where we made $\boldsymbol{\Sigma}^s$ tracefree by subtracting an isotropic tensor that only modifies the pressure, but does not affect the flow. Here, the distribution function Ψ is normalized such that:

$$\frac{1}{V} \int_{V} \int_{\Omega} \Psi(\mathbf{x}, \mathbf{n}, t) \, \mathrm{d}\mathbf{p} \, \mathrm{d}\mathbf{x} = n \tag{16}$$

where V is the volume of the system containing a total of N swimmers and $n = N/V$ is the mean number density in the suspension.

In this discussion, we have neglected contributions to the extra stress from the constraint forces appearing in Eqs. (7)–(8). In a dilute suspension where only swimmer-generated flows are accounted for, the single-particle contribution to the stress is indeed the dominant one. When there is an externally imposed flow (as when investigating rheology in Section 3), or when the swimmer density is high (as discussed in Section 4), the constraint forces must be accounted for in the extra stress and yield an additional stress contribution $\boldsymbol{\Sigma}^f$ expressed in terms of the fourth moment in $\mathbf{p}$ of the distribution function contracted against the rate-of-strain tensor; see Eq. (45). That said, when the swimmer concentration is high, our expression for the stress is not entirely consistent since the single swimmer model still assumes that the mean-field hydrodynamic velocity can be locally linearized and that near-field interactions with other swimmers need not be accounted for.

2.4. Basic kinetic model

We now have a closed system of equations for evolving the distribution of swimmer positions and orientations, which we recapitulate here in dimensionless form. The distribution function $\Psi(\mathbf{x}, \mathbf{p}, t)$ is evolved through the Smoluchowski equation:

$$\partial_t \Psi + \nabla_x \cdot (\dot{\mathbf{x}} \Psi) + \nabla_p \cdot (\dot{\mathbf{p}} \Psi) = 0 \tag{17}$$

where the fluxes in position and orientation are expressed as:

$$\dot{\mathbf{x}} = \mathbf{p} + \mathbf{u}(\mathbf{x}) - D \nabla_x \ln \Psi \tag{18}$$

$$\dot{\mathbf{p}} = (\mathbf{I} - \mathbf{pp}) \cdot \left[\beta \mathbf{E}(\mathbf{x}) + \mathbf{W}(\mathbf{x}) \right] \cdot \mathbf{p} - d \nabla_p \ln \Psi \tag{19}$$

Eqs. (17)–(19) are coupled to the forced Stokes equations for the mean-field (volume-averaged) pressure q and fluid velocity $\mathbf{u}$:

$$\nabla \cdot \mathbf{u} = 0, \qquad \nabla^2 \mathbf{u} - \nabla p = \nabla \cdot \boldsymbol{\Sigma}^s \tag{20}$$

where the flow is driven by the swimmer-generated active stress tensor:

$$\boldsymbol{\Sigma}^s(\mathbf{x}, t) = \alpha \int_{\Omega} \Psi(\mathbf{x}, \mathbf{p}, t)(\mathbf{pp} - \mathbf{I}/3) \, \mathrm{d}\mathbf{p} \tag{21}$$

Here, we have made the equations dimensionless by scaling space on a characteristic length l_c and time on V_0/l_c. Assuming that the system size is characterized by a linear scale L, so that the system volume is expressed as $V = L^3$, a natural choice of length scale is $l_c = \ell/\nu$, where $\nu = N\ell^3/L^3 = n\ell^3$ is an effective volume concentration of swimmers in the system. Upon this choice, the stresslet strength σ_0 characterizing the magnitude of the active particle stress is replaced with the purely geometric coefficient $\alpha = \pm \kappa_1/\kappa_2$. It is easy to see that this coefficient is negative for pusher particles ($\alpha < 0$), but positive for puller particles ($\alpha > 0$). It can be shown that α also provides a relation between the stresslet magnitude and swimming speed of a single swimmer as $\alpha = \sigma_0/\eta V_0 \ell^2$.

2.5. Mathematical aspects of the kinetic model

2.5.1. The relative conformational entropy

The difference that the swimmer type (pusher vs puller, as captured by the sign of α) makes in the dynamics is seen very directly in the evolution of the system's relative conformational entropy, which is an energy-like quantity defined by:

$$\mathscr{S}(t) = \iint\limits_{V \ \Omega} (\Psi/\Psi_0) \ln(\Psi/\Psi_0) \, d\mathbf{p} \, d\mathbf{x} \tag{22}$$

Here $\Psi_0 = 1/4\pi$ is the constant value of Ψ for a uniform and isotropic state. The entropy $\mathscr{S}(t)$ is non-negative, and is zero if and only if $\Psi \equiv \Psi_0$, so that departures of $\mathscr{S}$ from zero provide a global measure of the level of fluctuations away from uniform isotropy. The time derivative of the entropy obeys:

$$4\pi \dot{\mathscr{S}} = -\frac{6}{\alpha} \int\limits_V \mathbf{E} : \mathbf{E} \, d\mathbf{x} - \iint\limits_{V \ \Omega} \left[D|\nabla_x \ln \Psi|^2 + d|\nabla_p \ln \Psi|^2 \right] \Psi \, d\mathbf{p} \, d\mathbf{x} \tag{23}$$

The first term arises from the identity:

$$\int\limits_V 2\mathbf{E} : \mathbf{E} \, d\mathbf{x} = -\int\limits_V \mathbf{E} : \boldsymbol{\Sigma}^s \, d\mathbf{x} \tag{24}$$

which expresses the balance between the rate of viscous dissipation and the active power input to the system by swimming, and is easily derived by performing a mechanical energy balance on the Stokes equations (20). The second negative definite term arises from diffusive processes which serve to decrease the entropy. Note that if $\alpha < 0$, i.e. if the particles are pushers, then the first term on the right-hand side of Eq. (23) becomes positive and can drive $\mathscr{S}$ away from zero. When $\alpha > 0$, the active stress term is now negative definite and only serves to drive the system towards equilibrium in concert with the diffusive processes. The positivity of α, and decay of the conformational entropy, is shared by the extra stress generated by rotational thermal fluctuations in the theory of passive rod suspensions of Doi and Edwards [50].

2.5.2. Steady states and their stability

Two states of special importance in studying active suspensions are the aligned and isotropically ordered states. Aligned suspensions and their stability bear on questions of collective behaviors and flocking and were first considered in this context by Simha and Ramaswamy [42] using a phenomological theory for active nematics. Considering plane-wave perturbations of an aligned state, they concluded that for each perturbation wavelength there were perturbation wavevectors that gave rise to instability. This suggested that globally aligned steady states could not exist, at least in the Stokesian limit.

We also reexamined this question using the dilute kinetic model presented above [43,44]. For this, we sought special solutions of Eqs. (17) and (20), having set $D = d = 0$, where the distribution of swimming directions is everywhere concentrated as a Dirac delta function:

$$\Psi(\mathbf{x}, \mathbf{p}, t) = c(\mathbf{x}, t) \, \delta\big[\mathbf{p} - \mathbf{n}(\mathbf{x}, t)\big] \tag{25}$$

Here, $c(\mathbf{x}, t)$ is the local concentration and $\mathbf{n}(\mathbf{x}, t)$ the polar director field (or local swimming direction), both defined in Eq. (30) below. Both quantities are evolved by advective partial-differential equations derived without approximation from Eqs. (17) and (20). These equations support the globally aligned steady state $c \equiv 1$ and $\mathbf{n} \equiv \hat{\mathbf{z}}$, where $\hat{\mathbf{z}}$ is an arbitrary unit vector defining the direction of alignment. We considered plane-wave perturbations and derived a dispersion relation for two growth rates $\lambda_\pm$ as functions of the wavenumber k and of the angle θ of the perturbation wavevector from $\hat{\mathbf{z}}$:

$$\lambda_\pm = -\frac{\alpha}{4} f(\theta) \cos 2\theta \left[1 \pm \left(1 - \frac{8ik}{\alpha f(\theta)} \frac{\sin^2 \theta \cos \theta}{\cos^2 2\theta} \right)^{1/2} \right] \tag{26}$$

where $f(\theta) = (\beta + 1) \cos^2 \theta - (\beta - 1) \sin^2 \theta$. For $k > 0$ it is straightforward to show that λ_+ and λ_- have real parts of opposite sign regardless of swimmer type. This analysis then predicts that plane-wave perturbations are unstable for any choice of θ, k, or α. In the long-wave limit $k \to 0^+$ and for slender swimmers ($\beta = 1$), the growth rates become $\lambda_+ = -\alpha \cos^2 \theta \cos 2\theta$ and $\lambda_- = 0$, where λ_+ is the growth rate previously found by Simha and Ramaswamy [42]. Another important effect missing in this theory is rotational diffusion, which if included would yield temporal broadening of an initially sharply aligned state. In Section 4, we model steric interactions between swimmers, and show that at high concentrations these interactions can induce a local nematic alignment amongst swimmers that can balance the effect of rotational diffusion, yielding aligned states whose stability we then study [81].

In dilute suspensions, it is more relevant to analyze the stability of the isotropic, uniform state for which $\Psi = \Psi_0 = 1/4\pi$. The entropy analysis above suggests that this homogeneous state is globally attracting for suspensions of pullers (where $\alpha > 0$), but allows for instability for pushers. This expectation is borne out by linear stability analysis. Considering plane-wave perturbations of the homogeneous state leads to an integro-differential equation for the evolution of eigenmodes
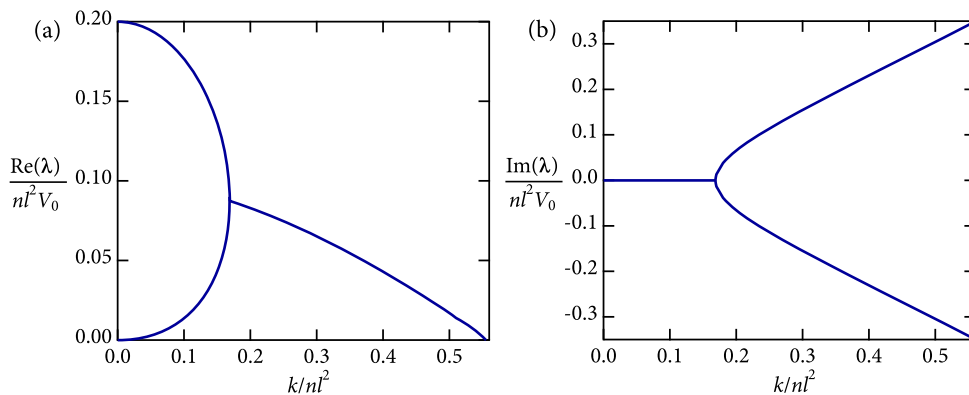
Fig. 3. The real (a) and imaginary (b) parts of the complex growth rate for a plane-wave perturbation to the state of uniform isotropy (i.e. $\Psi = \Psi_0 = 1/4\pi$) as a function of the normalized perturbation wave number k. In the normalizations, l is the swimmer length, V_0 the swimmer speed, and n the mean swimmer number density. Adapted from Ref. [44].

upon the unit sphere of orientations [43,44,82]. An important simplification follows from observing that the active stress that drives instability contributes to the eigenmode evolution only through the first azimuthal mode upon the sphere [82]. All other eigenmodes are damped or neutrally stable. This suggests that this instability, at least in the linear regime, will drive local nematic alignment, and a physical mechanism for this effect was proposed by Subramanian and Koch [46], who noted that the hydrodynamic flow resulting from a weak nematic perturbation to particle orientations tends to further reinforce the perturbation via Jeffery's equation in the case of pushers.

Fig. 3 shows the computed real and imaginary parts of the normalized growth rates for a suspension of pushers near uniform isotropy, as functions of the normalized wavelength of perturbation [43,44]. Here, translational and rotational diffusion have been neglected, though it is straightforward to see that translational diffusion only modifies the growth rates by an amount of $-Dk^2$. At very long waves, the real part shows a double-branched structure that collapses to a single branch at shorter length scales, which is coincident with the imaginary part becoming double-branched and non-zero. The single branch of unstable growth-rates ceases to exist upon crossing the k-axis for $k > k_c$, with $k_c \approx 0.56$ [82]. In the absence of diffusive processes, these graphs are universal as the only remaining parameter, α, can be set to ± 1 (that is, up to its sign) by rescaling space and time by $|\alpha|$.

Hohenegger and Shelley [82] studied the linear system further by using asymptotic methods to investigate the nature of solutions for $k \gg 1$ where solutions to the growth-rate eigenvalue problem do not exist, while also demonstrating that rotational diffusion restores the existence of the negative branch while shifting it down in value. Finally, by assuming that the rotational diffusion of swimming particles scales linearly with particle concentration, and that translational diffusion scales inversely, as is consistent with Brenner's generalized Taylor dispersion theory [83] and with our numerical simulations based on slender-body theory in the semi-dilute regime [40], they predicted that homogeneous suspensions of pushers would be unstable to large-scale hydrodynamic flows if

$$\frac{L}{\ell}\nu > K \tag{27}$$

and stable otherwise. Here, K is a constant depending upon the diffusion scalings and on the details of swimmer actuation and shape. This criterion therefore predicts instability if either the system size L (normalized by the swimmer length ℓ) or the effective volume concentration of swimmers $\nu = n\ell^3$ becomes sufficiently large. This criterion was confirmed qualitatively in numerical simulations of many interacting motile rods [41], and is also consistent with the current experimental evidence [10].

One very important aspect of the linear stability analysis is that it does not predict the growth of concentration fluctuations. Indeed, concentration fluctuations are predicted to decay as a result of translational diffusion. However, it is the orientational instability that drives the system into the nonlinear regime where concentration fluctuations then appear. It is to this regime that we now turn.

2.6. The nonlinear dynamics of active suspensions

As a computational model, Eqs. (17) and (20) are quite challenging to evolve. In three dimensions, there are three independent positional variables corresponding to the spatial coordinates (x, y, z), and two orientational variables for the parameterization of the orientation vector **p**. For this reason, highly resolved simulations have been restricted to two dimensions with one angle of orientation [43,44]. Nonetheless, fully three-dimensional simulations are possible using multiprocessor computing [81,84,85], though with resolutions that are modest relative to the two-dimensional case.

One such three-dimensional simulation is shown in Fig. 4(a), which for triply periodic boundary conditions shows the swimmer concentration field for a suspension of pushers ($\alpha = -1$) that begins in a state of near uniform isotropy. As
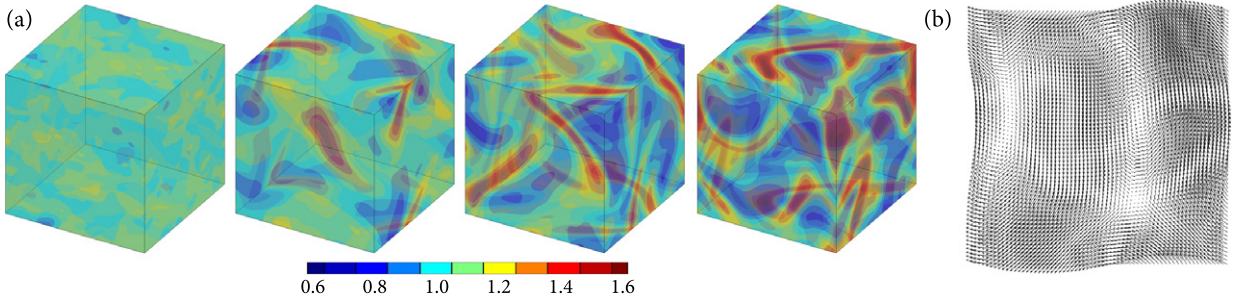
Fig. 4. (a) The evolution of the three-dimensional concentration field for a suspension of pushers, beginning near the state of uniform isotropy. (b) The background fluid velocity in a slice across the computational box. The simulations were obtained using the simulation method of Alizadeh Pahlavan and Saintillan [84].

predicted by the linear theory, there is growth away from homogeneity manifested first by increased local orientational order. As the flow becomes more nonlinear, concentration fluctuations appear in the form of sheets of relatively high swimmer concentration. The growth of concentration fluctuations, which does not occur in the linear regime, can be attributed to a source term of the form $-c\nabla \cdot \mathbf{n}$ in the equation for the concentration field (see Eq. (32) below), which can cause swimmers to aggregate spatially as a result of their swimming velocity [44]. While persistently observed, these sheets are transitory and show continual folding, stretching, and reformation. Fig. 4(b) shows the background fluid velocity, calculated from Eq. (20), in a slice across the computational volume: velocity fields in unstable pusher suspensions are unsteady and chaotic, and strongly correlated on the scale of the system as can be expected based on the linear stability results of Fig. 3, where the longest wavelength is always expected to be the most unstable. Unsurprisingly perhaps, these complex flows emerging in pushers suspensions have very good mixing properties, as we previously characterized in our two-dimensional kinetic simulations [44] and in our three-dimensional many-particle simulations of swimming rods [41].

The roots of the persistent flow instability for pushers can be seen in Eq. (24), which shows the balance of swimmer input power with the rate of viscous dissipation. We expand this equation as

$$\int_V 2\mathbf{E} : \mathbf{E} \, d\mathbf{x} = -\alpha \int_V \int_\Omega (\mathbf{pp} : \mathbf{E}) \, \Psi(\mathbf{x}, \mathbf{p}, t) \, d\mathbf{p} \, d\mathbf{x} \tag{28}$$

Hence, the local active power density is given by

$$p(\mathbf{x}, t) = -\alpha \int_\Omega (\mathbf{pp} : \mathbf{E}) \, \Psi(\mathbf{x}, \mathbf{p}, t) \, d\mathbf{p} \tag{29}$$

which, for $\alpha < 0$, will be maximized when swimmers are oriented in the direction of maximal fluid rate of strain. However, it is a property of Jeffery's equation (6) that slender rods rotate toward the direction of maximal strain rate, and it is through this propensity that suspensions of pushers continuously power the growth of fluctuations. Though not shown here, the configurational entropy $\mathscr{S}(t)$ in simulations shows initial growth from being nearly zero, and eventually achieves saturated quasi-oscillatory dynamics that reflect a balance between the growth of fluctuations and their destruction by diffusive processes [44]. As already implied, similar simulations of puller suspensions show monotonic decay of both the entropy and input power towards zero.

2.7. Approximations and extensions

2.7.1. Moment equations and closure approximations

To circumvent the complexity arising from the high-dimensionality of the kinetic model of Section 2.4, a number of approximate models have been derived that rely on equations for orientational moments of the distribution function Ψ. Of particular interest are the zeroth, first, and second moments, which correspond respectively to the concentration field $c(\mathbf{x}, t)$, polar order parameter $\mathbf{n}(\mathbf{x}, t)$, and nematic order parameter $\mathbf{Q}(\mathbf{x}, t)$ defined as follows:

$$c(\mathbf{x}, t) = \langle 1 \rangle, \qquad \mathbf{n}(\mathbf{x}, t) = \frac{\langle \mathbf{p} \rangle}{c(\mathbf{x}, t)}, \qquad \mathbf{Q}(\mathbf{x}, t) = \frac{\langle \mathbf{pp} - \mathbf{I}/3 \rangle}{c(\mathbf{x}, t)} \tag{30}$$

where $\langle \cdot \rangle$ denotes the orientational average:

$$\langle h(\mathbf{p}) \rangle = \int_\Omega h(\mathbf{p}) \, \Psi(\mathbf{x}, \mathbf{p}, t) \, d\mathbf{p} \tag{31}$$

Evolution equations for c, $\mathbf{n}$, and $\mathbf{Q}$ are readily obtained by taking moments of the Smoluchowski equation (1):

$$D_t c = -\nabla \cdot (c\mathbf{n}) + D\nabla^2 c \tag{32}$$

$$D_t (c\mathbf{n}) = -\big[\nabla \cdot (c\mathbf{Q}) + (1/3)\nabla c\big] + D\nabla^2 (c\mathbf{n}) + \big(c\mathbf{In} - \langle\mathbf{ppp}\rangle\big) : (\beta\mathbf{E} + \mathbf{W}) - 2dc\mathbf{n} \tag{33}$$

$$D_t (c\mathbf{Q}) = -\big[\nabla \cdot \langle\mathbf{ppp}\rangle - (\mathbf{I}/3)\nabla \cdot (c\mathbf{n})\big] + D\nabla^2 (c\mathbf{Q}) + \beta c\big[\mathbf{E} \cdot (\mathbf{Q} + \mathbf{I}/3) + (\mathbf{Q} + \mathbf{I}/3) \cdot \mathbf{E}\big]$$
$$+ c[\mathbf{W} \cdot \mathbf{Q} - \mathbf{Q} \cdot \mathbf{W}] - 2\beta\langle\mathbf{pppp}\rangle : \mathbf{E} - 6dc\mathbf{Q} \tag{34}$$

where $D_t \equiv \partial_t + \mathbf{u} \cdot \nabla$ is the material derivative. Also note that the hydrodynamic velocity $\mathbf{u}$, and the rate-of-strain tensor $\mathbf{E}$ and the vorticity tensor $\mathbf{W}$ depend on the nematic order parameter $\mathbf{Q}$ via the active stress tensor $\boldsymbol{\Sigma}^s = \alpha c\mathbf{Q}$ forcing the Stokes equations (20). Unsurprisingly, the system of Eqs. (32)–(34) also involves higher moments of the distribution function, and specifically its third and fourth moments $\langle\mathbf{ppp}\rangle$ and $\langle\mathbf{pppp}\rangle$. To close the system, these two moments must be expressed in terms of c, $\mathbf{n}$, and $\mathbf{Q}$ by means of closure approximations. Several closure models have been proposed in the context of liquid crystals and particle suspensions, and we present of few of them here.

One of the simplest closure model perhaps can be interpreted as a severely truncated expansion of the distribution function Ψ on the basis of spherical harmonics:

$$\Psi(\mathbf{x}, \mathbf{p}, t) \approx \frac{c(\mathbf{x}, t)}{4\pi}\bigg[1 + 3\mathbf{p} \cdot \mathbf{n}(\mathbf{x}, t) + \frac{15}{2}\mathbf{pp} : \mathbf{Q}(\mathbf{x}, t)\bigg] \tag{35}$$

in which the coefficients of all harmonics of degree 3 and higher are neglected. By calculating third- and fourth-order moments of Eq. (35), this can be shown to be equivalent to the following closure relations for $\langle\mathbf{ppp}\rangle$ and $\langle\mathbf{pppp}\rangle$, in index notation:

$$\langle p_i p_j p_k \rangle \approx \frac{c}{5}(n_i \delta_{jk} + n_j \delta_{ik} + n_k \delta_{ij}) \tag{36}$$

$$\langle p_i p_j p_k p_l \rangle \approx \frac{c}{15}(\delta_{ij}\delta_{kl} + \delta_{ik}\delta_{jl} + \delta_{il}\delta_{jk}) + \frac{c}{7}(\delta_{ij}Q_{kl} + \delta_{ik}Q_{jl} + \delta_{il}Q_{jk} + \delta_{jk}Q_{il} + \delta_{jl}Q_{ik} + \delta_{kl}Q_{ij}) \tag{37}$$

where we see that the closure corresponds to linear approximations of $\langle\mathbf{ppp}\rangle$ and $\langle\mathbf{pppp}\rangle$ in terms of $\mathbf{n}$ and $\mathbf{Q}$, respectively. Substituting these expressions in Eqs. (33)–(34) for $\mathbf{n}$ and $\mathbf{Q}$ then yields closed evolution equations, which can be used for analysis or simulations. This closure model was used by Baskaran and Marchetti [47] in their model for the hydrodynamics of bacterial suspensions, and a variant was also recently applied by Brotto et al. [86] to study instabilities in confined active suspensions in two-dimensions. Note, however, that the truncation of Eq. (35) does not depend on the flow field at all (even though particle orientations are affected by it through Jeffery's equation), and is only a good approximation if the distribution function Ψ is nearly isotropic.

Other types of closures have been proposed for the fourth moment $\langle\mathbf{pppp}\rangle$. First, Doi [49] suggested a quadratic dependence of the fourth moment on the second moment as

$$\langle p_i p_j p_k p_l \rangle \approx \frac{1}{c}\langle p_i p_j \rangle\langle p_k p_l \rangle = c(Q_{ij} + \delta_{ij}/3)(Q_{kl} + \delta_{kl}/3) \tag{38}$$

This model has been commonly used in theories for passive and active liquid crystals, e.g. [49,87–92]. However, the approximation of Eq. (38) is clearly *ad hoc* and does not originate from a self-consistent solution for the orientation distribution or from a consideration of the local flow field. A more rigorous approach was adopted by Hinch and Leal [93] in the context of passive Brownian suspensions. Hinch and Leal derived the following composite approximation for $\langle\mathbf{pppp}\rangle : \mathbf{E}$ based on asymptotic solutions for the orientation distribution in the weak and strong flow limits:

$$\langle\mathbf{pppp}\rangle \approx \frac{1}{5}\big[6\langle\mathbf{pp}\rangle \cdot \mathbf{E} \cdot \langle\mathbf{pp}\rangle - \langle\mathbf{pp}\rangle\langle\mathbf{pp}\rangle : \mathbf{E} - 2\mathbf{I}\langle\mathbf{pp}\rangle^2 : \mathbf{E} + 2\mathbf{I}\langle\mathbf{pp}\rangle : \mathbf{E}\big] \tag{39}$$

where the second moment $\langle\mathbf{pp}\rangle$ appearing on the right-hand side is then related to the nematic order parameter as $\langle\mathbf{pp}\rangle = c(\mathbf{Q} + \mathbf{I}/3)$. A model based on this approach was recently used by Woodhouse and Goldstein [94] in two dimensions to model an apolar suspension of active filaments ($\mathbf{n} \equiv \mathbf{0}$), where spontaneous circulation was predicted to emerge under confinement as a result of activity.

2.7.2. Run-and-tumble dynamics of wild-strain bacteria

The motion of motile bacteria, such as *Escherichia coli* and *Bacillus subtilis*, not only involves swimming as a result of self-propulsion and transport by the local fluid flow, but is also affected by their so-called run-and-tumble dynamics, by which periods of directed swimming ("runs") are interspersed by random reorientation events ("tumbles") resulting from the rapid unbundling and rebundling of their flagella [95,96]. As will be discussed in Section 5, these tumbling events, which occur with a characteristic rate λ, play a central role in chemotaxis, or the ability of bacteria to migrate towards or away from chemical cues or nutrients in the suspending fluid. As discussed by Subramanian and Koch [46], who derived a kinetic model very similar to that of Section 2.4, these run-and-tumble dynamics are well approximated as a Poisson process with frequency λ, which modifies the Smoluchowski equation as
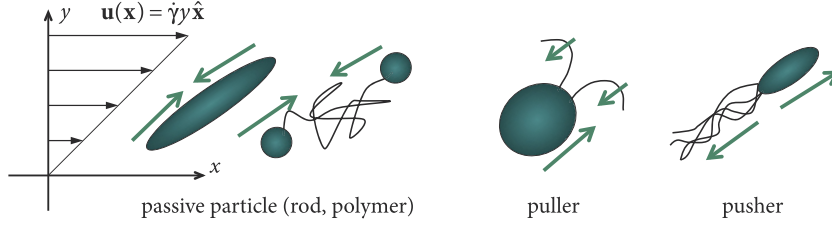
Fig. 5. Basic mechanism for the effect of activity on the effective viscosity of a suspension of particles in shear flow (after Hatwalne et al. [97]). In the case of passive particles (rods, polymers), the flow induces a dipole that tends to resist stretching. The permanent dipole due to swimming is of the same sign for pullers, but of opposite sign for pushers.

$$\partial_t \Psi + \nabla_x \cdot (\dot{\mathbf{x}} \Psi) + \nabla_p \cdot (\dot{\mathbf{p}} \Psi) = -\lambda(\mathbf{x}, \mathbf{p}, t)\Psi + \int_\Omega \lambda(\mathbf{x}, \mathbf{p}', t)\, K(\mathbf{p}, \mathbf{p}')\Psi(\mathbf{x}, \mathbf{p}', t)\, d\mathbf{p}' \tag{40}$$

In this equation, the first term on the right-hand side models bacteria that tumble away from orientation $\mathbf{p}$ with characteristic frequency $\lambda(\mathbf{x}, \mathbf{p}, t)$, whereas the second term models bacteria that tumble from orientation $\mathbf{p}'$ to $\mathbf{p}$ with frequency $\lambda(\mathbf{x}, \mathbf{p}', t)$. The function $K(\mathbf{p}, \mathbf{p}')$, or "turning kernel", captures the correlation between pre- and post-tumble orientations. Indeed, the average change in orientation for *Escherichia coli* is approximately 68.5°, indicating a correlation in the forward direction [46,95]. Subramanian and Koch [46] proposed the following form for the turning kernel:

$$K(\mathbf{p}, \mathbf{p}') = \frac{B e^{B(\mathbf{p} \cdot \mathbf{p}')}}{4\pi \sinh B} \tag{41}$$

where the parameter B characterizes the correlation in orientation. In the limit of $B \to 0$, $K = 1/4\pi$ and pre- and post-tumble orientations are completely uncorrelated. In the absence of any chemoattractant (or repellant), the tumbling rate assumes a constant value λ_0 that is independent of $\mathbf{x}$ and $\mathbf{p}$; when chemotaxis occurs, such a dependency may arise and will be discussed in more detail in Section 5. The effect of particle tumbling on the instability of the isotropic uniform state discussed in Section 2.5.2 was also analyzed by Subramanian and Koch [46], who showed that it has a stabilizing effect on the dynamics at all wavenumbers much like orientational diffusion, and can give rise to an intrinsic critical volume fraction for instability that no longer depends on system size.

3. Rheology and external flows

A simple and direct consequence of the active stress derived in Section 2.3 is that it modifies the effective rheology of a suspension of active particles in an external flow. This was first recognized by Hatwalne et al. [97], who proposed the simple mechanism illustrated in Fig. 5. In an imposed shear flow, an elongated particle subject to diffusion undergoes tumbling dynamics [56] but assumes a mean orientation close to the flow direction in the first flow quadrant. In the case of a passive particle, such as a rigid rod or a flexible polymer, the extensional component of the flow tries to stretch the particle, which resists by exerting a contractile force dipole on the flow that effectively increases the viscosity of the suspension, especially at low shear rates; this contractile force dipole can be understood from the flow-induced constraint forces appearing in Eqs. (7)–(8) in the model of Section 2.1 for a slender rigid rod. In the case of an active particle, this effect still persists, but in addition the particle exerts a permanent dipole due to swimming, whose sign depends on the swimming mechanism. In the case of a puller, the swimming dipole is of the same sign as the flow-induced dipole (contractile), whereas a pusher exerts a permanent dipole of opposite sign (extensile). As a result, we expect a further increase in viscosity in puller suspensions (with respect to a suspension of passive particles of the same shape), whereas a decrease in viscosity is expected in suspensions of pushers.

A number of models with various levels of complexity have been constructed to calculate the effective viscosity of such suspensions in the dilute regime, e.g. [60,61]. Here, we describe the simple theory of Saintillan [98,99] for shear and extensional rheology, which extends previous classical work on passive suspensions of rodlike particles [93,100–102] and also evaluates normal stresses. As can be anticipated from the mechanism described in Fig. 5, a key component of the theory is the determination of the orientation distribution of the particles in the imposed external flow, from which the stress tensor is obtained in terms of orientation moments as described below. If interactions between particles can be neglected (for instance in the dilute limit), the configuration of the suspension is simply represented by an orientation distribution function $\Psi(\mathbf{p}, t)$, which satisfies a simplified Smoluchowski equation:

$$\partial_t \Psi + \nabla_p \cdot (\dot{\mathbf{p}} \Psi) = 0 \tag{42}$$

where Ψ is now normalized as

$$\int_\Omega \Psi(\mathbf{p}, t)\, d\mathbf{p} = 1 \tag{43}$$
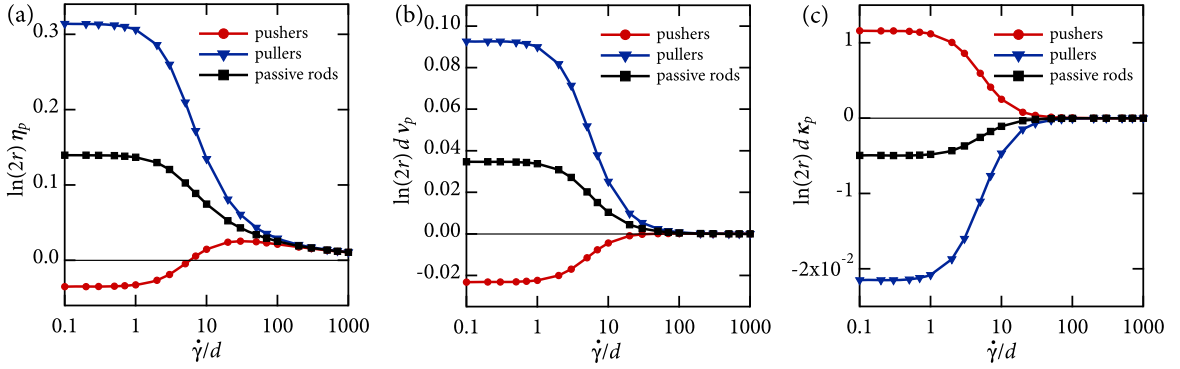
Fig. 6. Shear rheology of an active suspension (adapted with permission from Saintillan [98]): (a) intrinsic viscosity, (b) first and (c) second normal stress difference coefficients, as functions of shear rate $\dot{\gamma}$ for a rodlike particle of aspect ratio r. Some of the variables are made dimensionless using the rotary diffusivity d. The plot shows results for passive particles ($\sigma_0 = 0$), pushers ($\sigma_0 < 0$), and pullers ($\sigma_0 > 0$).

In Eq. (42), particle rotations result from the external flow with rate-of-strain and vorticity tensors $\mathbf{E}_0$ and $\mathbf{W}_0$, respectively:

$$\dot{\mathbf{p}} = (\mathbf{I} - \mathbf{pp}) \cdot (\beta \mathbf{E}_0 + \mathbf{W}_0) \cdot \mathbf{p} - d\nabla_p \ln \Psi \tag{44}$$

Here, we focus on the steady-state orientation distribution, which is simply obtained by setting $\dot{\mathbf{p}} = \mathbf{0}$. In extensional flows, an exact analytical solution for $\Psi(\mathbf{p})$ can be obtained [99,103]; such is not the case in simple shear flow, where either numerical solutions [98,104] or approximate asymptotic solutions in the limit of weak or strong flows can be derived [93].

Once the steady orientation distribution is known, it is used to evaluate the particle extra stress in the suspension as $\boldsymbol{\Sigma}^p = \boldsymbol{\Sigma}^f + \boldsymbol{\Sigma}^b + \boldsymbol{\Sigma}^s$, where the three stress contributions arise from the external flow (constraint forces in Eqs. (7)–(8)), Brownian rotations (in the case of colloidal particles), and the permanent dipole due to swimming. These stress tensors are evaluated in a similar fashion as in Section 2 by taking a configurational average of the force dipoles (or stresslets) exerted by the particles on the flow [78,80], and can be expressed as:

$$\boldsymbol{\Sigma}^f = nA\left[\langle \mathbf{pppp}\rangle - \frac{\mathbf{I}}{3}\langle\mathbf{pp}\rangle\right] : \mathbf{E}_0, \qquad \boldsymbol{\Sigma}^f = nkT\left[\langle\mathbf{pp}\rangle - \frac{\mathbf{I}}{3}\right], \qquad \boldsymbol{\Sigma}^s = n\sigma_0\left[\langle\mathbf{pp}\rangle - \frac{\mathbf{I}}{3}\right] \tag{45}$$

In Eq. (45), the various stress tensors are found to depend only on the second and fourth moments of $\Psi(\mathbf{p})$; n denotes the mean number density, kT is the thermal energy of the fluid, and A is a constant depending on the shape of the particles that can be evaluated as $A = \pi\eta\ell^3/6\ln(2r)$ for a slender particle of length ℓ and aspect ratio r [51,79]. Once the stress tensor has been calculated, the intrinsic viscosity η_P, as well as the first and second normal stress difference coefficients ν_P and κ_P are easily obtained. For instance, in a shear flow of the form $\mathbf{u}(\mathbf{x}) = \dot{\gamma}\, y\hat{\mathbf{x}}$:

$$\eta_P = \frac{\Sigma_{xy}^p}{n\ell^3\eta\dot{\gamma}}, \qquad \nu_P = \frac{\Sigma_{xx}^p - \Sigma_{yy}^p}{n\ell^3\eta\dot{\gamma}^2}, \qquad \kappa_P = \frac{\Sigma_{yy}^p - \Sigma_{zz}^p}{n\ell^3\eta\dot{\gamma}^2} \tag{46}$$

where $n\ell^3$ denotes the effective volume fraction. Results for η_P, ν_P and κ_P in a simple shear flow are plotted in Fig. 6 as functions of imposed shear rate $\dot{\gamma}$, for pushers, pullers, and passive rodlike particles. Suspensions of passive rods exhibit shear thinning, a positive first normal stress difference and negative second normal stress difference. The effects of activity are strongest at low shear rates, where the intrinsic viscosity increases in suspensions of pullers but decreases for pushers, in agreement with the basic mechanism of Fig. 5. In suspensions of pushers, this can even result in a negative intrinsic viscosity at low shear rates. An analytical expression for the zero-shear-rate intrinsic viscosity can be derived as [98]:

$$\eta_P^0 = \lim_{\dot{\gamma}\to 0} \eta_P(\dot{\gamma}) = \frac{1}{15}(1 + 3\beta) + \frac{\beta\ln(2r)\sigma_0}{5\pi\eta\ell^3 d} \tag{47}$$

where the first term on the right-hand side is the zero-shear-rate viscosity in a suspension of passive rods, and the second term arises from activity and is linear in the active stresslet strength σ_0. The effect of activity is also visible in the normal stress difference coefficients, which are enhanced for pullers, but change sign in the case of pushers. Qualitatively similar trends are also observed in irrotational extensional flows [99].

Detailed experimental measurements of the effective rheology have been scarce but qualitatively support the results of the dilute theory. Two significant hurdles in these measurements are the low viscosity of the suspending fluid (typically water) and the low shear rates at which the effects of activity manifest themselves. Sokolov and Aranson [105] considered suspensions of *Bacillus subtilis*, a pusher bacterium, and used a clever technique based on the rotation of a magnetically actuated rotor placed in a free-standing film of a bacterial suspension. By measuring the viscous torque on the particle, they inferred the effective viscosity of the suspension, which was found to be less than the viscosity of the fluid in the dilute regime, but was found to increase again at higher concentrations. The case of pullers was addressed by Rafaï et al. [106],

who performed conventional rheometry on suspensions of the micro-alga *Chlamydomonas reinhardtii* over a wide range of concentrations, and found a net increase in viscosity with respect to a suspension of dead cells at the same volume fraction. More recently, Gachelin et al. [107] devised a microfluidic rheometer based on the deflection of the interface between two coflowing streams of a suspension of *Escherichia coli* and of clear fluid in a Y-shaped channel. The results they reported on the effective viscosity were once again consistent with Fig. 6(a): they observed a negative intrinsic viscosity in weak flows (at least in the dilute limit), followed by a maximum of the viscosity at an intermediate value of $\dot{\gamma}$ and finally by a shear-thinning regime in strong flows. Normal stresses in either pusher or puller suspensions have yet to be measured experimentally.

The theory described above, as well as other related models, has focused on the dilute limit where hydrodynamic interactions between particles are negligible. Attempts at understanding the effects of such interactions in the semi-dilute regime have used direct numerical simulations based on simplified swimmer models. Ishikawa and Pedley [36] performed Stokesian dynamics simulations of sheared suspensions of spherical squirmers that swim as a result of a prescribed slip velocity on their surface. In the case of non-bottom-heavy squirmers, they found no effect of activity on the viscosity; this is easily understood as there is no mechanism for such particles to assume an anisotropic orientation distribution. In the case of bottom-heavy squirmers, which are subject to a buoyancy torque, anisotropic orientations become possible and a non-Newtonian rheology was observed, including non-zero normal stress differences. More recently, Berlyand and coworkers [62,63,108] performed direct numerical simulations of collections of model elongated swimmers representing bacteria. They noted that hydrodynamic interactions between particles result in an effective noise which plays the same role as rotational diffusion in the model described above, and observed a decrease in viscosity in the dilute regime, followed by an increase as volume fraction further increases, in agreement with the experimental observations of Sokolov and Aranson [105]. One key question, which has yet to be addressed in detail, is the precise influence of the large-scale collective motions arising in semi-dilute suspensions on the rheology. Understanding this influence requires modeling of the effect of the external flow on collective motion. This point was addressed both theoretically and computationally within the kinetic framework of Section 2 by Alizadeh Pahlavan and Saintillan [84], who found that an external shear flow has a stabilizing effect on the instability and chaotic dynamics observed in quiescent suspensions as a result of the alignment of the particles in the flow.

A number of studies have also focused on the rheology of active liquid crystals (polar or apolar) and active gels [92,109–113], which share many similarities with active suspensions. These studies are typically based on evolution equations for the polar and nematic order parameters $\mathbf{n}(\mathbf{x}, t)$ and $\mathbf{Q}(\mathbf{x}, t)$, such as the equations presented in Section 2.7.1. In addition, these models often include nematic elasticity, which captures local nematic alignment as a result of steric interactions between particles as discussed next in Section 4. Similar findings have been reported within this framework, including negative intrinsic viscosities and oppositely-signed normal stress differences in contractile systems. Additional interesting effects have also been described, such as hysteresis [112,113] and shear-banding [92].

4. Modeling concentration effects

The basic kinetic model described in Section 2 focuses on long-ranged hydrodynamic interactions between particles, and demonstrates that such interactions can lead to instabilities and the emergence of coherent structures in sufficiently concentrated active suspensions. In experiments on bacterial suspensions, collective motion is also observed to only occur if the volume fraction is sufficiently high [7,9,114]; however, at such volume fractions, steric interactions resulting from direct contacts between particles are significant and can hardly be neglected. This was noted by Cisneros et al. [114], who observed a transition to local directional order and pattern formation in concentrated suspensions of bacteria. The importance of steric interactions is also very clear in swarming experiments, where bacterial colonies are allowed to grow on agar substrates [115–117]: in such experiments, long-ranged hydrodynamic interactions are likely negligible, but correlated motions in the form of large swirls and jets are still observed and must be primarily a consequence of near-field steric effects. This raises the question of the respective roles of hydrodynamic and steric interactions in the collective dynamics of concentrated active suspensions.

In passive suspensions of Brownian rodlike particles and liquid crystals, it is well known that increasing concentration results in a transition from an isotropic state to a nematic state in which particles align locally with their neighbors as steric interactions overcome the randomizing effect of rotary diffusion [50,118]. At the particle level, this transition can be explained as an entropic effect, as the effective volume taken up by a particle in the isotropic phase is larger than in the nematic phase, and a simple scaling based on this argument suggests that the transition should occur when $nb\ell^2 \sim O(1)$, where b and ℓ are the characteristic thickness and length of a particle, respectively. In suspensions of active swimmers, such as rod-shaped bacteria, a similar effect is also expected to take place and is likely to have an influence on the dynamics.

In continuum models for active liquid crystals and active gels, the effect of steric interactions is generally accounted for by means of a free energy resulting from distortions from the uniformly aligned state. Phenomenological expressions for the free energy can be constructed based on symmetry arguments. In nematics, the Landau–de Gennes free energy $\mathscr{F}$ is commonly used [88,89,118,119], and more specifically its one-constant approximation with density given by:

$$f = \frac{K}{2} \partial_k Q_{ij} \partial_k Q_{ij}$$ (48)

This free energy modifies the evolution equation for the nematic order parameter $\mathbf{Q}$ (for instance Eq. (34) together with one of the closure models discussed in Section 2.7.1) by addition of a term of the form $\Gamma \mathbf{H}$ on the right-hand side, where Γ is

a constant modeling collective rotational diffusion, and the second-order tensor **H** is the so-called molecular field obtained from the free energy as:

$$H_{ij} = -\frac{\partial \mathscr{F}}{\partial Q_{ij}} + \frac{\delta_{ij}}{3}\frac{\partial \mathscr{F}}{\partial Q_{kk}} \tag{49}$$

A vectorial molecular field can also be constructed and added to the evolution equation for the polar order parameter **n** in the case of a polar liquid crystal [120,121].

The kinetic model of Section 2 can also be modified to account for steric interactions. One such extension was attempted in nearly two-dimensional geometries by Aranson et al. [122], who described steric effects based on a pairwise collision operator, which has the effect of aligning two swimming particles coming into contact. The form of this operator is motivated by experimental observations of *Bacillus subtilis* in thin liquid films, where two colliding cells are found to subsequently swim as a pair. One significant difficulty in this formulation is that a correct description of these interactions involves the pair probability distribution function in the suspension, which in the model of Aranson et al. is approximated as the product of two singlet distributions. Aranson et al. are then able to derive moment equations for the concentration c and polar order parameter **n**, from which a Landau-type bifurcation is predicted for the order parameter above a critical volume fraction.

More recently, Ezhilan et al. [81] proposed a more direct extension of the kinetic theory of Section 2 for concentrated suspensions, in which steric interactions are captured using a mean-field model inspired by the Doi and Edwards theory for the isotropic-to-nematic transition [50]. Precisely, steric interactions are modeled by means of an additional torque in Eq. (19) for the angular flux, causing particles to align locally:

$$\dot{\mathbf{p}} = (\mathbf{I} - \mathbf{pp}) \cdot (\beta\mathbf{E} + \mathbf{W}) \cdot \mathbf{p} - \nabla_p \mathscr{U}(\mathbf{x}, \mathbf{p}, t) - d\nabla_p \ln\Psi \tag{50}$$

The interaction potential $\mathscr{U}$ is expressed as:

$$\mathscr{U}(\mathbf{x}, \mathbf{p}, t) = \int_\Omega \Psi(\mathbf{x}, \mathbf{p}', t) U(\mathbf{p}, \mathbf{p}') \, d\mathbf{p}' \tag{51}$$

where a convenient choice of the kernel U is given by the Maier–Saupe potential [123]: $U(\mathbf{p}, \mathbf{p}') = -U_0(\mathbf{p} \cdot \mathbf{p}')^2$. Using these expressions for $\mathscr{U}$ and U, it is easy to rewrite Eq. (50) in the simple form:

$$\dot{\mathbf{p}} = (\mathbf{I} - \mathbf{pp}) \cdot (\beta\mathbf{E} + \mathbf{W} + 2U_0 c\mathbf{Q}) \cdot \mathbf{p} - d\nabla_p \ln\Psi \tag{52}$$

It is clear from this form that the effect of the steric torque at every point in space is to align the particles nematically with the principal axis of the nematic order parameter tensor **Q**, which corresponds to the local preferred direction of alignment. In addition to this simple modification, the particle stress tensor in concentrated suspensions must also be modified: two additional stress contributions arising from the inextensibility of the particles in the flow they generate and from the steric torques on the particles must also be accounted for and can be evaluated based on slender-body theory in the case of a high-aspect-ratio particle [50,81] (E. Lushi has also developed a numerical method for suspensions of interacting discrete swimmers that accounts for steric interactions and for this extra stress contribution; personal communication). Both of these stress tensors can be shown to depend quadratically on volume fraction, unlike the active stress that has a linear dependence.

The leading effect of the steric torque is to drive the isotropic-to-nematic transition when the dimensionless parameter $\xi = 2U_0 n/d$ (where n is the number density) comparing the strength of steric interactions to rotary diffusion is increased. Specifically, two types of uniform steady base states of the form $\Psi(\mathbf{x}, \mathbf{p}, t) = \Psi_0(\mathbf{p})$ can be solved for by setting the angular flow $\dot{\mathbf{p}}$ in Eq. (52) to zero: the isotropic base state $\Psi_0(\mathbf{p}) = n/4\pi$ is always an exact solution of the equations, but at sufficiently high values of ξ two additional axisymmetric nematic base states also exist, which are both of the form

$$\Psi_0(\mathbf{p}) = \Psi(\theta) = C\exp[\delta(\xi)\cos 2\theta] \tag{53}$$

where C is a normalization constant. In Eq. (53), θ is the angle between **p** and the direction of nematic alignment, which is indeterminate. The coefficient $\delta(\xi)$ can be obtained by solving a nonlinear equation [81], which has two non-zero solutions corresponding to the nematic states only when $\xi \gtrsim 13.46$. A full linear stability analysis of these various base states was performed by Ezhilan et al. [81], and the stability results are illustrated in Fig. 7 for pushers ($\alpha < 0$), pullers ($\alpha > 0$), and movers ($\alpha = 0$, i.e. particles that swim without exerting any active stress). In the case of movers, the isotropic base state is found to be stable up to $\xi = 15$; of the two nematic states, one is always unstable, and the second one, which is also the most energetically favorable, is weakly unstable as a result of the steric stress tensor, though this state is likely to be stabilized by translational diffusion in real systems. Active stresses in suspensions of pushers are destabilizing, and all branches are found to become unstable before the isotropic-to-nematic transition even occurs. Pullers, however, have a stabilizing effect: the isotropic state has the same stability as in the case of movers, and one of the nematic states is stable over a finite range of ξ near the nematic transition, but becomes unstable at high values of ξ. This last result differs fundamentally from the dilute case discussed in Section 2, in which suspensions of pullers were found to be always stable. In both suspensions of movers and pullers, there exists a range of values of ξ near the transition over which both isotropic
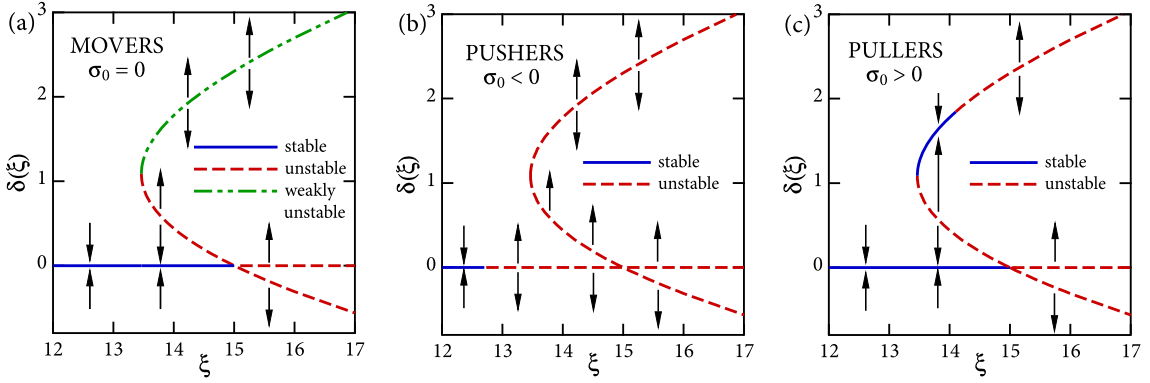
Fig. 7. Stability of the isotropic ($\delta(\xi) = 0$) and nematic ($\delta(\xi) \neq 0$) base states as a function of $\xi = 2U_0 n/d$, according to the analysis of Ezhilan et al. [81]. Results are shown for: (a) movers (i.e. particles that swim but do not exert an active stress), (b) pushers, and (c) pullers.
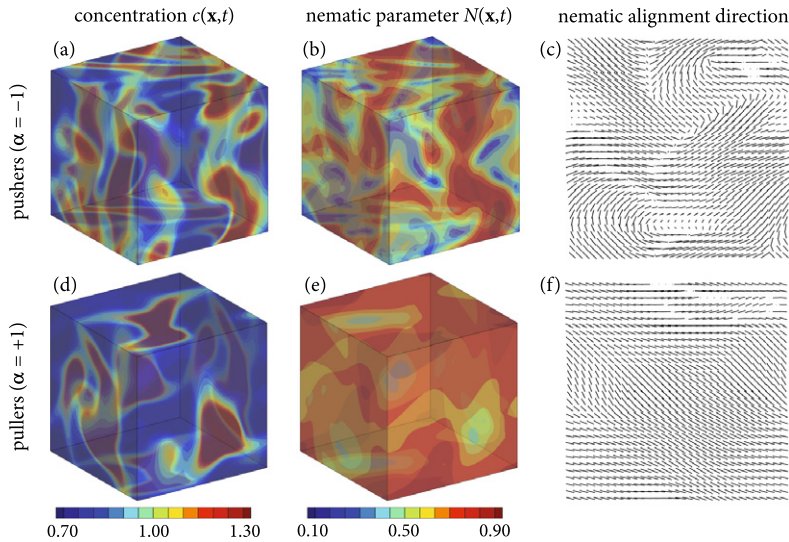
Fig. 8. Nonlinear simulations of the dynamics in concentrated active suspensions (adapted with permission from Ezhilan et al. [81]): (a)–(c) show results for the concentration field $c(\mathbf{x}, t)$, nematic parameter $N(\mathbf{x}, t)$ (defined as $3e_Q/2$ where e_Q is the largest eigenvalue of $\mathbf{Q}$), and nematic alignment direction (defined as the direction of the eigenvector of $\mathbf{Q}$ with eigenvalue e_Q) in the case of pushers ($\alpha = -1$); (d)–(f) show the same quantities in the case of pullers ($\alpha = +1$). Both simulations were obtained for $\xi = 2U_0 n/d = 26.92$.

and nematic states are stable: as previously discussed by Doi and Edwards [50], this may result in hysteresis or phase separation.

Ezhilan et al. [81] also confirmed the results of this stability analysis by three-dimensional fully nonlinear simulations of the kinetic equations in a periodic domain. These simulations support the predictions of the stability analyses, and typical patterns observed in the nonlinear regime in unstable pusher and puller suspensions are illustrated in Fig. 8. Unstable pusher suspensions show very similar patterns and dynamics as in the dilute regime, and the leading effect of steric interactions is to enhance local particle alignment. The case of unstable puller suspensions is, however, distinct: the morphology of the observed patterns is different, and the dynamics are found to be significantly slower than in pusher suspensions at the same volume fraction.

The models discussed above highlighted the important effect of steric interactions on the dynamics in concentrated active suspensions, where direct contacts between particles tend to cause them to align. However, other effects not captured by these theories are also expected to come into play: at very high concentrations, describing velocities in the fluid and particle phases in terms of a single velocity field $\mathbf{u}(\mathbf{x}, t)$ is likely inaccurate, and a more realistic theory would account for both phases separately, for instance using a two-fluid model. Such models have been developed successfully to describe concentrated suspensions of inert particles [124–126]; a first attempt at describing active suspensions in this manner is due to Wolgemuth [45], though more work remains to be done in this area.

5. Chemotaxis

Bacteria rarely evolve in idealized environments in which they only interact via hydrodynamic (and possibly steric) interactions: they often grow and develop in confined spaces where they also interact with chemical cues or seek oxygen and nutrients. Understanding how chemotaxis (or directed motion of bacteria towards or away from a chemical species) is affected by hydrodynamics and mixing by self-induced flows is therefore an important problem for the modeling of chemical transport and communication in bacterial suspensions, and likely bears consequences on more complex phenomena such as biofilm formation. A clear experimental study of some of these effects was performed by Sokolov et al. [10], who studied the dynamics of suspensions of the bacterium *Bacillus subtilis* in thin free-standing liquid films, where oxygen was free to diffuse from the boundaries into the suspension. They were able to image the bacterial concentration profiles across the film thickness, and made the following observations. In very thin films (with thickness $L \lesssim 100$ μm), they found that the concentration profile reached a steady state with a fairly weak migration of the bacteria towards the interfaces where oxygen concentration is the highest. As film thickness was increased ($L \gtrsim 200$ μm), a transition to three-dimensional chaotic motion was found to occur, with much stronger migration towards the surfaces, and unsteady plumes of bacteria penetrating into the bulk and enhancing transport.

The directed migration of swimming bacteria such as *Escherichia coli* or *Bacillus subtilis* along a chemical gradient is achieved as a result of their run-and-tumble dynamics introduced in Section 2.7.2. Bacteria are able to modulate the characteristic frequency λ of their tumbling events according to experienced changes in concentration of a chemoattractant (or repellant), which results in an effective biased random walk in the direction of the gradient. In the case of a chemoattractant (such as oxygen or a nutrient), the tumbling rate is observed to decrease (with respect to its base value λ_0 in the absence of a gradient) as a bacterium is moving towards regions of high concentration, and increase otherwise; these dynamics are reversed in the case of a repellant. The precise dependence of the tumbling rate on the concentration $s(\mathbf{x}, t)$ of the chemical cue was studied experimentally by Brown and Berg [127], who measured the following relation in the case of *Escherichia coli*:

$$\ln \lambda = \ln \lambda_0 - C \dot{P}_b \tag{54}$$

where C is a constant and P_b is the fractional amount of bound chemoreceptors, which, at low concentrations, is expected to be proportional to the chemoattractant concentration in solution. In cases where the concentration varies with both space and time (for instance when the chemoattractant field is being mixed by the swimmers), this suggests the following form for the stopping rate:

$$\lambda = \lambda_0 \exp(-\zeta \mathscr{D}_t s) \tag{55}$$

where ζ is the chemotactic response strength and $\mathscr{D}_t s$ is a Lagrangian derivative capturing the rate of change of the chemoattractant concentration s as experienced by a bacterium moving with velocity $V_0 \mathbf{p} + \mathbf{u}$:

$$\mathscr{D}_t s = \partial_t s + (V_0 \mathbf{p} + \mathbf{u}) \cdot \nabla s \tag{56}$$

A linearized version of Eq. (55) in the limit where $|\zeta \mathscr{D}_t s| \ll 1$ has also been used [128]: $\lambda = \lambda_0 (1 - \zeta \mathscr{D}_t s)$, which further simplifies to $\lambda = \lambda_0 (1 - \zeta V_0 \mathbf{p} \cdot \nabla s)$ in the case of a constant and uniform gradient in s and in the absence of a mean-field hydrodynamic flow.

Motivated by the experiments of Sokolov et al. [10], several recent studies have considered the case of chemotaxis in an externally imposed gradient of a chemoattractant such as oxygen. Koch and coworkers [129,130] focused on linear stability analyses in the case where the oxygen field is prescribed and is not affected by the flow, which is a good approximation if the oxygen Péclet number is high. First, Subramanian et al. [129] considered the case of an infinite suspension of run-and-tumble bacteria in a constant and uniform oxygen gradient, which they analyzed using a model very similar to the one described here. They first noted that the run-and-tumble dynamics result in an anisotropic orientation distribution, with a net polar alignment in the direction of the gradient. They then performed a linear stability analysis, where they found that chemotaxis has a destabilizing effect and tends to reduce the critical bacterial concentration for instability that they had previously derived in the absence of the tumbling bias [46]. More recently, Kasyap and Koch [130] examined a situation closely related to that of the experiments of Sokolov et al. [10]: they analyzed theoretically the stability of a confined suspension of run-and-tumble bacteria when a chemoattractant gradient is prescribed in the direction of confinement. By assuming that the full distribution function can be approximated as the product of a density field $c(\mathbf{x}, t)$ and of an orientation distribution $\psi(\mathbf{p}, t)$, and using lubrication theory for the fluid flow inside the film, they predicted a long-wavelength instability in which active stresses drive flows that tend to reinforce density fluctuations in the plane of the film.

The effects of oxygen transport and of nonlinearities were recently modeled by Ezhilan et al. [85], who simulated the full nonlinear kinetic and flow equations of Section 2 coupled to an advection–diffusion–reaction equation for the chemical concentration field $s(\mathbf{x}, t)$:

$$\partial_t s + \mathbf{u}(\mathbf{x}, t) \cdot \nabla s - D_0 \nabla^2 s = -\kappa c(\mathbf{x}, t) s(\mathbf{x}, t) \tag{57}$$

Here, the chemoattractant (for instance oxygen) is transported by the flow, diffuses, and is consumed by the bacteria according to a second-order reaction. Simulations were performed in a doubly-periodic thin film geometry, with a free-shear-stress
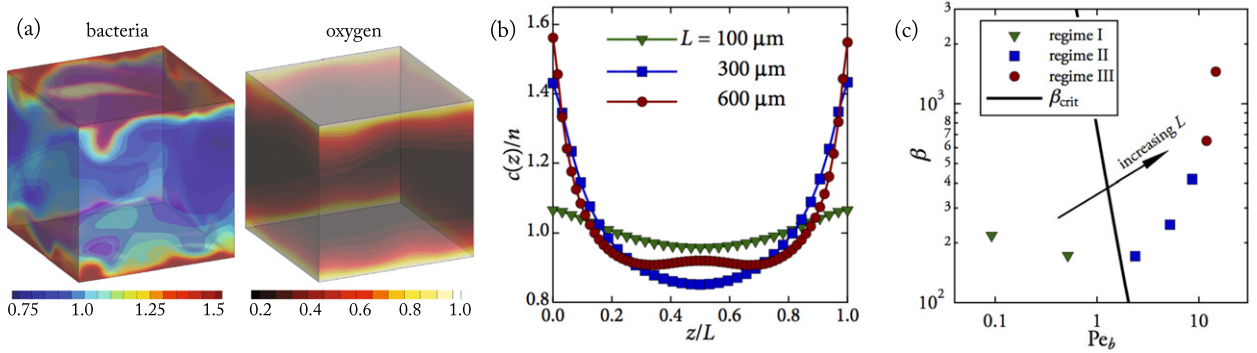
Fig. 9. Dynamics in thin films of aerotactic bacteria (adapted with permission from Ezhilan et al. [85]): (a) bacterial and oxygen concentration fields in a film of thickness $L = 600$ μm in the unstable regime; (b) average bacterial concentration profiles in films of various thicknesses; (c) comparison to the results of the linear stability analysis of Kasyap and Koch [130], which predicts an instability when $\beta = -3\Sigma_{zz}L/2\eta U_d$ exceeds a critical value β_{crit} expressed in terms of $Pe_b = 3LU_d\lambda_0/V_0^2$ (where $U_d = V_0 \int p_z \Psi \, d\mathbf{p}$ is the aerotactic drift velocity).

condition for the velocity field on the boundaries, and a no-flux condition for the concentration field. Ezhilan et al. observed dynamics quite similar to the experimental findings of Sokolov et al. [10], as illustrated in Fig. 9. In particular, both bacteria and oxygen were found to approach steady concentration profiles in thin films; above a critical film thickness, a transition to three-dimensional chaotic dynamics was observed, in which dense plumes of bacteria penetrated the bulk of the film as shown in Fig. 9(a), thereby enhancing both bacterial and oxygen transport and mixing. In very thick films, a dense bacterial layer was also observed near the centerline in agreement with experiments, and was attributed to the nearly uniform oxygen concentration in this region, where chemotaxis ceases. The onset of instability in these nonlinear simulations was compared to the linear stability analysis of Kasyap and Koch [130], and showed favorable agreement as illustrated in Fig. 9(c).

A different situation arises when the chemoattractant is secreted by the swimming bacteria themselves, as was recently modeled by Lushi et al. [131]. Their study was motivated by previous studies of bacterial self-concentration as a result of chemotactic focusing [132], as well as communication processes in bacterial colonies via quorum sensing [133,134]. This situation was studied in the past using the celebrated Keller–Segel model [135] and its many variants [136–138], though these models had all neglected the effect of the fluid flow generated by the swimmers. As discussed by Lushi et al., a transport equation similar to Eq. (57) can be used in this case:

$$\partial_t s + \mathbf{u}(\mathbf{x}, t) \cdot \nabla s - D_0 \nabla^2 s = -b_1 s(\mathbf{x}, t) + b_2 c(\mathbf{x}, t) \tag{58}$$

where the consumption term on the right-hand-side has been replaced by two first-order reaction terms for chemoattractant degradation (with rate constant b_1) and production by the bacteria (with rate constant b_2).

One steady state for this system is uniform isotropy for the swimmers, with a balance of production and degradation in the chemoattractant concentration. Linearizing around this state for a simplified version of the model, Lushi et al. found two uncoupled stability problems for chemotactically-driven aggregation and alignment-driven large-scale flows. As a function of tumbling frequency, they identified different regimes where instabilities to aggregation, or alignment, or both, are dominating.

The nonlinear development of these instabilities is illustrated in Fig. 10 from near steady-state uniformity. The bare dynamics of a suspension undergoing chemotactic aggregation without hydrodynamic coupling (i) shows a pattern of coarsening into larger and larger aggregates. Curiously, chemotactic pullers (ii) also show an initial aggregation which is then stopped at a particular length scale. The resulting near-circular aggregates appear to be mutually repelling through the development of small-scale hydrodynamic flows. Finally, (iii) shows chemotactic pushers for system parameters where hydrodynamic flows are suppressed, at least near steady state, but where the system is unstable to aggregation. What is seen here is that aggregation can drive swimmer concentration up and induce locally unstable flows. Unlike the first two cases, the flows are now highly dynamic and fragmented. One central lesson from this study seems to be that the intrinsic flows generated by swimmers can limit the self-aggregation. In very recent work, Lushi et al. [139] also found very similar dynamics in a chemotaxis model for swimmers that execute turns, rather tumbles, in response to chemotactic sensing.

6. Concluding remarks

Biologically active suspensions have generated much excitement over the last decade in several research communities, from biology and physics to engineering and applied mathematics. The complexity of the dynamics and patterns that emerge in these systems as a result of seemingly simple interactions are quite fascinating, and a variety of mathematical models have been developed to elucidate the origin of these phenomena. As is apparent from this review, these models are based on simplifying assumptions, which can be viewed as either a strength or a limitation: on the one hand, they allow one to explore the roles of the different types of interactions between swimmers, while on the other hand they will never fully
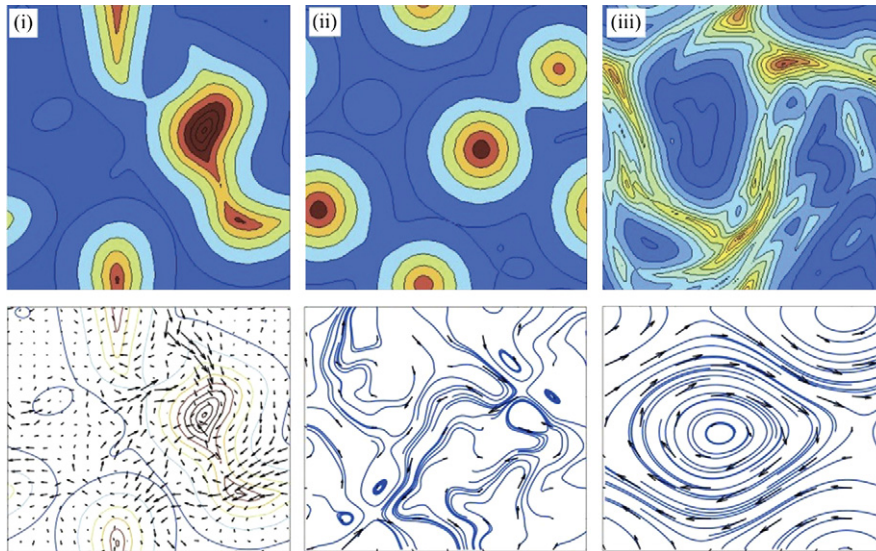
Fig. 10. Structure and dynamics of swimmer concentration in chemotactic suspensions at long times. (i) is for chemotactic swimmers without hydrodynamic interactions; (ii) is for chemotactic pullers; (iii) is for chemotactic pushers. Lower figures are corresponding flow streamlines and polar order parameter **n**. Reproduced with permission from Lushi et al. [131].

capture all of the effects at play in biological experiments, which often also involve complex chemistry and signaling. On the experimental side, the prospect of using synthetic autonomous microswimmers [16,17,19,20,140,141] such as chemically powered nanorods may offer an opportunity to test predictions from kinetic theories and other models more quantitatively, though such swimmers have yet to be deployed in large enough numbers to undergo collective motion.

It is interesting to recall the close analogy between active suspensions and a number of other active biophysical systems, including: actin–myosin beds [29] and networks [142], cytoskeletal networks [27], motor-protein–microtubule complexes [26], to name a few. In all of these systems, individual components have the ability to draw energy from their environment (generally in the form of ATP) and to convert it to mechanical energy by exerting forces on their surroundings (other particles, medium, or substrate). When the components of the system also have the ability to move and orient, either autonomously or as a result of interactions or fluid flow, collective dynamics often ensues as in the case of active suspensions. It is quite remarkable how similar the mechanisms and models for the dynamics in these varied systems can be, and this has prompted researchers in these areas to classify them under the general label of "soft active matter" [143,144].

While much of the research work, both experimental and theoretical, in the area of active suspensions and related biophysical and artificial systems has been fundamental in character, the curious behavior of these suspensions is likely to bring about a wealth of technological applications. The ability of bacteria to efficiently mix fluid in the absence of inertia has previously been reported in microfluidic flows [13], and the non-Newtonian rheology and mechanical behavior of these suspensions, notably their ability to reduce the apparent viscosity of the suspending fluid, is also quite unusual though it has yet to be exploited in engineering devices. Another natural though technically challenging use of these systems consists in harnessing the mechanical energy imparted by active swimmers on their surroundings to perform engineering tasks: for instance, the ability to use bacteria to pump fluid [145], power gears [146,147], transport and assemble micron-sized objects [148], has already been demonstrated.

Acknowledgements

References

[1] E. Lauga, T.R. Powers, The hydrodynamics of swimming microorganisms, Rep. Prog. Phys. 72 (2009) 096601.
[2] E.W. Knight-Jones, Relation between metachronism and the direction of ciliary beat in Metazoa, Q. J. Microsc. Sci. 95 (1954) 503–521.
[3] K.-I. Okamoto, Y. Nakaoka, Reconstitution of metachronal waves in ciliated cortical sheets of *Paramecium*. I. Wave stabilities, J. Exp. Biol. 192 (1994) 61–72.
[4] X.-L. Wu, A. Libchaber, Particle diffusion in a quasi-two-dimensional bacterial bath, Phys. Rev. Lett. 84 (2000) 3017–3020.
[5] C. Dombrowski, L. Cisneros, S. Chatkaew, R.E. Goldstein, J.O. Kessler, Self-concentration and large-scale coherence in bacterial dynamics, Phys. Rev. Lett. 93 (2004) 098103.

[6] I. Tuval, L. Cisneros, C. Dombrowski, C.W. Wolgemuth, J.O. Kessler, R.E. Goldstein, Bacterial swimming and oxygen transport near contact lines, Proc. Natl. Acad. Sci. USA 102 (2005) 2277–2282.

[7] L.H. Cisneros, R. Cortez, C. Dombrowski, R.E. Goldstein, J.O. Kessler, Fluid dynamics of self-propelled microorganisms, from individuals to concentrated populations, Exp. Fluids 43 (2007) 737–753.

[8] N.H. Mendelson, A. Bourque, K. Wilkening, K.R. Anderson, J.C. Watkins, Organized cell swimming motions in *Bacillus subtilis* colonies: patterns of short-lived whirls and jets, J. Bacteriol. 181 (1999) 600–609.

[9] A. Sokolov, I.S. Aranson, J.O. Kessler, R.E. Goldstein, Concentration dependence of the collective dynamics of swimming bacteria, Phys. Rev. Lett. 98 (2007) 158102.

[10] A. Sokolov, R.E. Goldstein, F.I. Feldchtein, I.S. Aranson, Enhanced mixing and spatial instability in concentrated bacterial suspensions, Phys. Rev. E 80 (2009) 031903.

[11] G.V. Soni, B.M. Jaffar Ali, T. Hatwalne, G.V. Shivashankar, Single particle tracking of correlated bacterial dynamics, Biophys. J. 84 (2003) 2634–2637.

[12] Q. Liao, G. Subramanian, M.P. DeLisa, D.L. Koch, M. Wu, Pair velocity correlations among swimming *Escherichia coli* bacteria are determined by force-quadrupole hydrodynamic interactions, Phys. Fluids 19 (2007) 061701.

[13] M.J. Kim, K.S. Breuer, Enhanced diffusion due to motile bacteria, Phys. Fluids 16 (2004) 78–81.

[14] K.C. Leptos, J.S. Guasto, J.P. Gollub, A.I. Pesci, R.E. Goldstein, Dynamics of enhanced tracer diffusion in suspensions of swimming eukaryotic microorganisms, Phys. Rev. Lett. 103 (2009) 198103.

[15] H. Kurtuldu, J.S. Guasto, K.A. Jonhson, J.P. Gollub, Enhancement of biomixing by swimming algal cells in two dimensions, Phys. Rev. Lett. 108 (2011) 10391–10395.

[16] S.J. Ebbens, J.R. Howse, In pursuit of propulsion at the nanoscale, Soft Matter 6 (2010) 726–738.

[17] W.F. Paxton, K.C. Kistler, C.C. Olmeda, A. Sen, S.K. St. Angelo, Y. Cao, T.E. Mallouk, P.E. Lammert, Catalytic nano motors: autonomous movement of striped nanorods, J. Am. Chem. Soc. 126 (2004) 13424–13431.

[18] W.F. Paxton, A. Sen, T.E. Mallouk, Motility of catalytic nanoparticles through self-generated forces, Eur. J. Chem. 11 (2005) 6462–6470.

[19] J.R. Howse, R.A.L. Jones, A.J. Ryan, T. Gough, R. Vafabakhsh, R. Golestanian, Self-motile colloidal particles: from directed propulsion to random walk, Phys. Rev. Lett. 99 (2007) 048102.

[20] J.L. Moran, P.M. Wheat, J.D. Posner, Locomotion of electrocatalytic nanomotors due to reaction induced charge autoelectrophoresis, Phys. Rev. E 81 (2010) 065302.

[21] R. Laocharoensuk, J. Burdick, J. Wang, Carbon-nanotube-induced acceleration of catalytic nanomotors, ACS Nano 2 (2008) 1069–1075.

[22] R. Dreyfus, J. Baudry, M.L. Roper, H.A. Stone, M. Fermigier, J. Bibette, Microscopic artificial swimmers, Nature 437 (2005) 862–865.

[23] D. Zerrouki, J. Baudry, D. Pine, P. Chaiken, J. Bibette, Chiral colloidal clusters, Nature 455 (2008) 380.

[24] A. Ghosh, P. Fischer, Controlled propulsion of artificial magnetic nanostructured propellers, Nano Lett. 9 (6) (2009) 2243–2245.

[25] L. Zhang, J.J. Abbott, L. Dong, B.E. Kratochvil, D. Bell, B.J. Nelson, Artificial bacterial flagella: Fabrication and magnetic control, Appl. Phys. Lett. 94 (2009) 064107.

[26] T. Surrey, F. Nédélec, S. Leibler, E. Karsenti, Physical properties determining self-organization of motors and microtubules, Science 292 (2001) 1167–1171.

[27] S. Köhler, V. Schaller, A.R. Bausch, Collective dynamics of active cytoskeletal networks, PLoS ONE 6 (2011) 23798.

[28] T. Sanchez, D. Chen, S. DeCamp, M. Heymann, Z. Dogic, Spontaneous motion in hierarchically assembled active matter, Nature 491 (2012) 431–435.

[29] V. Schaller, C. Weber, C. Semmrich, E. Frey, A.R. Bausch, Polar patterns of driven filaments, Nature 467 (2010) 73–77.

[30] Y. Sumino, K. Nagai, Y. Shitaka, D. Tanaka, K. Yoshikawa, H. Chate, K. Oiwa, Large-scale vortex lattice emerging from collectively moving microtubules, Nature 483 (2012) 448–452.

[31] J.P. Hernandez-Ortiz, C.G. Stoltz, M.D. Graham, Transport and collective dynamics in suspensions of confined swimming particles, Phys. Rev. Lett. 95 (2005) 204501.

[32] K. Drescher, R.E. Goldstein, N. Michel, M. Polin, I. Tuval, Direct measurement of the flow field around swimming microorganisms, Phys. Rev. Lett. 105 (2010) 168101.

[33] J.S. Guasto, K.A. Johnson, J.P. Gollub, Oscillatory flows induced by microorganisms swimming in two dimensions, Phys. Rev. Lett. 105 (2010) 168102.

[34] K. Drescher, J. Dunkel, L.H. Cisneros, S. Ganguly, R.E. Goldstein, Fluid dynamics and noise in bacterial cell–cell and cell–surface scattering, Proc. Natl. Acad. Sci. USA 108 (2011) 10940–10945.

[35] J.P. Hernández-Ortiz, P.T. Underhill, M.D. Graham, Dynamics of confined suspensions of swimming particles, J. Phys. Condens. Matter 21 (2009) 204107.

[36] T. Ishikawa, T.J. Pedley, The rheology of a semi-dilute suspension of swimming model micro-organisms, J. Fluid Mech. 588 (2007) 399–435.

[37] T. Ishikawa, J.T. Locsei, T.J. Pedley, Fluid particle diffusion in a semidilute suspension of model micro-organisms, Phys. Rev. E 82 (2010) 021408.

[38] T. Ishikawa, T.J. Pedley, Coherent structures in monolayers of swimming particles, Phys. Rev. Lett. 100 (2008) 088103.

[39] T. Ishikawa, J.T. Locsei, T.J. Pedley, Development of coherent structures in concentrated suspensions of swimming model micro-organisms, J. Fluid Mech. 615 (2008) 401–431.

[40] D. Saintillan, M. Shelley, Orientational order and instabilities in suspensions of self-locomoting rods, Phys. Rev. Lett. 99 (2007) 058102.

[41] D. Saintillan, M. Shelley, Emergence of coherent structures and large-scale flows in motile suspensions, J. R. Soc. Interface 9 (2012) 571.

[42] R.A. Simha, S. Ramaswamy, Hydrodynamic fluctuations and instabilities in ordered suspensions of self-propelled particles, Phys. Rev. Lett. 89 (2002) 058101.

[43] D. Saintillan, M. Shelley, Instabilities and pattern formation in active particle suspensions: Kinetic theory and continuum simulations, Phys. Rev. Lett. 100 (2008) 178103.

[44] D. Saintillan, M. Shelley, Instabilities, pattern formation and mixing in active suspensions, Phys. Fluids 20 (2008) 123304.

[45] C. Wolgemuth, Collective swimming and the dynamics of bacterial turbulence, Biophys. J. 95 (2008) 1564.

[46] G. Subramanian, D.L. Koch, Critical bacterial concentration for the onset of collective swimming, J. Fluid Mech. 632 (2009) 359–400.

[47] A. Baskaran, M.C. Marchetti, Statistical mechanics and hydrodynamics of bacterial suspensions, Proc. Natl. Acad. Sci. USA 106 (2009) 15567–15572.

[48] H. Wensinka, J. Dunkel, S. Heidenreich, K. Drescher, R. Goldstein, H. Lowen, J. Yeomans, Meso-scale turbulence in living fluids, Proc. Natl. Acad. Sci. USA 109 (2012) 14308–14313.

[49] M. Doi, Molecular dynamics and rheological properties of concentrated solutions of rodlike polymers in isotropic and liquid crystalline phases, J. Polym. Sci., Polym. Phys. Ed. 19 (1981) 229–243.

[50] M. Doi, S.F. Edwards, The Theory of Polymer Dynamics, Oxford University Press, Oxford, 1986.

[51] G.K. Batchelor, Slender-body theory for particles of arbitrary cross-section in Stokes flow, J. Fluid Mech. 44 (1970) 419–440.

[52] J. Keller, S. Rubinow, Slender-body theory for slow viscous flow, J. Fluid Mech. 75 (1976) 705–714.

[53] R.E. Johnson, An improved slender-body theory for Stokes flow, J. Fluid Mech. 99 (1980) 411–431.

[54] C. Hohenegger, M. Shelley, Dynamics of complex bio-fluids, in: M. Ben-Amar, A. Goriely, M. Muller, L. Cugliandolo (Eds.), New Trends in the Physics and Mechanics of Biological Systems, Oxford University Press, 2011.

[55] G.B. Jeffery, The motion of ellipsoidal particles immersed in a viscous fluid, Proc. R. Soc. Lond. A 102 (1922) 161–179.

[56] F.P. Bretherton, The motion of rigid particles in a shear flow at low Reynolds number, J. Fluid Mech. 14 (1962) 284–304.

[57] M. Garcia, S. Berti, P. Peyla, S. Rafaï, Random walk of a swimmer in a low-Reynolds-number medium, Phys. Rev. E 83 (2011) 035301.
[58] P.T. Underhill, J.P. Hernandez-Ortiz, M.D. Graham, Diffusion and spatial correlations in suspensions of swimming particles, Phys. Rev. Lett. 100 (2008) 248101.
[59] P.T. Underhill, M.D. Graham, Correlations and fluctuations of stress and velocity in suspensions of swimming microorganisms, Phys. Fluids 23 (2011) 121902.
[60] B.M. Haines, I.S. Aranson, L. Berlyand, D.A. Karpeev, Effective viscosity of dilute bacterial suspensions: A two-dimensional model, Phys. Biol. 5 (2008) 046003.
[61] B.M. Haines, A. Sokolov, I.S. Aranson, L. Berlyand, D.A. Karpeev, Three-dimensional model for the effective viscosity of bacterial suspensions, Phys. Rev. E 80 (2009) 041922.
[62] V. Gyrya, K. Lipnikov, I.S. Aranson, L. Berlyand, Effective shear viscosity and dynamics of suspensions of micro-swimmers from small to moderate concentrations, J. Math. Biol. 62 (2011) 707–740.
[63] S.D. Ryan, B.M. Haines, L. Berlyand, F. Ziebert, I.S. Aranson, Viscosity of bacterial suspensions: Hydrodynamic interactions and self-induced noise, Phys. Rev. E 83 (2011) 050904.
[64] A. Decoene, S. Martin, B. Maury, Microscopic modeling of active bacterial suspensions, Math. Model. Nat. Phenom. 6 (2011) 98–129.
[65] M.J. Lighthill, On the squirming motion of nearly spherical deformable bodies through liquids at very small Reynolds numbers, Commun. Pure Appl. Math. 5 (1952) 109–118.
[66] J.R. Blake, A spherical envelope approach to ciliary propulsion, J. Fluid Mech. 46 (1971) 199–208.
[67] V. Magar, T. Goto, T.J. Pedley, Nutrient uptake by a self-propelled steady squirmer, Q. J. Mech. Appl. Math. 56 (2003) 65–91.
[68] V. Magar, T.J. Pedley, Average nutrient uptake by a self-propelled unsteady squirmer, J. Fluid Mech. 539 (2005) 93–112.
[69] A. Kanevsky, M. Shelley, A.-K. Tornberg, Modeling simple locomotors in Stokes flow, J. Comput. Phys. 229 (2010) 958–977.
[70] J. Happel, H. Brenner, Low Reynolds Number Hydrodynamics with Special Applications to Particulate Media, Springer, 1983.
[71] C. Brennen, H. Winet, Fluid mechanics of propulsion by cilia and flagella, Annu. Rev. Fluid Mech. 9 (1977) 339–398.
[72] M.B. Short, C.A. Solari, S. Ganguly, T.R. Powers, J.O. Kessler, R.E. Goldstein, Flows driven by agella of multicellular organisms enhance long-range molecular transport, Proc. Natl. Acad. Sci. USA 103 (2006) 8315–8319.
[73] H. Lamb, Hydrodynamics, Dover, 1932.
[74] T. Ishikawa, M.P. Simmonds, T.J. Pedley, Hydrodynamic interaction of two swimming model micro-organisms, J. Fluid Mech. 568 (2006) 119–160.
[75] A.A. Evans, T. Ishikawa, T. Yamaguchi, E. Lauga, Instabilities and global order in concentrated suspensions of spherical microswimmers, Phys. Fluids 23 (2011) 111702.
[76] S. Spagnolie, E. Lauga, Hydrodynamics of self-propulsion near a boundary: Predictions and accuracy of far-field approximations, J. Fluid Mech. 700 (2012) 105–147.
[77] L. Zhu, M. Do-Quang, E. Lauga, L. Brandt, Locomotion by tangential deformation in a polymeric fluid, Phys. Rev. E 83 (2011) 011901.
[78] G.K. Batchelor, The stress system in a suspension of force-free particles, J. Fluid Mech. 41 (1970) 545–570.
[79] G.K. Batchelor, The stress generated in a non-dilute suspension of elongated particles by pure straining motion, J. Fluid Mech. 46 (1971) 813–829.
[80] G.K. Batchelor, Transport properties of two-phase materials with random structure, Annu. Rev. Fluid Mech. 6 (1974) 227–255.
[81] B. Ezhilan, M.J. Shelley, D. Saintillan, Instabilities and nonlinear dynamics of concentrated active suspensions, submitted for publication.
[82] C. Hohenegger, M. Shelley, Stability of active suspensions, Phys. Rev. E 81 (2010) 046311.
[83] H. Brenner, A general theory of Taylor dispersion phenomena, Physicochem. Hydrodyn. 1 (1980) 91–123.
[84] A. Alizadeh Pahlavan, D. Saintillan, Instability regimes in flowing suspensions of swimming micro-organisms, Phys. Fluids 23 (2011) 011901.
[85] B. Ezhilan, A. Alizadeh Pahlavan, D. Saintillan, Chaotic dynamics and oxygen transport in thin films of aerotactic bacteria, Phys. Fluids 24 (2012) 091701.
[86] T. Brotto, J.-B. Caussin, E. Lauga, D. Bartolo, Hydrodynamics of confined active fluids, Phys. Rev. Lett. 110 (2013) 038101.
[87] B.J. Edwards, A.N. Beris, M. Grmela, Generalized constitutive equation for polymeric liquid crystals. Part 1. Model formulation using the Hamiltonian (Poisson bracket) formulation, J. Non-Newton. Fluid Mech. 35 (1990) 51–72.
[88] A.N. Beris, B.J. Edwards, Thermodynamics of Flowing Systems, Oxford University Press, Oxford, 1994.
[89] M.E. Cates, O. Heinrich, D. Marenduzzo, K. Stratford, Lattice Boltzmann simulations of liquid crystalline fluids: Active gels and blue phases, Soft Matter 5 (2009) 3791–3800.
[90] D. Marenduzzo, E. Orlandini, M.E. Cates, J.M. Yeomans, Steady-state hydrodynamic instabilities of active liquid crystals: Hybrid lattice-Boltzmann simulations, Phys. Rev. E 76 (2007) 031921.
[91] D. Marenduzzo, E. Orlandini, Hydrodynamics of non-homogeneous active gels, Soft Matter 6 (2010) 774–778.
[92] S.M. Fielding, D. Marenduzzo, M.E. Cates, Nonlinear dynamics and rheology of active fluids: Simulations in two dimensions, Phys. Rev. E 83 (2011) 041910.
[93] E.J. Hinch, L.G. Leal, Constitutive equations in suspension mechanics. Part 2. Approximate forms for a suspension of rigid particles affected by Brownian rotations, J. Fluid Mech. 76 (1976) 187–208.
[94] F.G. Woodhouse, R.E. Goldstein, Spontaneous circulation of confined active suspensions, Phys. Rev. Lett. 109 (2012) 168105.
[95] H.C. Berg, Random Walks in Biology, Princeton University Press, 1983.
[96] H.C. Berg, D.A. Brown, Chemotaxis in *Escherichia coli* analysed by three-dimensional tracking, Nature 239 (1972) 500–504.
[97] Y. Hatwalne, S. Ramaswamy, M. Rao, R. Aditi Simha, Rheology of active-particle suspensions, Phys. Rev. Lett. 92 (2004) 118101.
[98] D. Saintillan, The dilute rheology of swimming suspensions: A simple kinetic model, Exp. Mech. 50 (2010) 1275–1281.
[99] D. Saintillan, Extensional rheology of active suspensions, Phys. Rev. E 81 (2010) 056307.
[100] H. Brenner, Rheology of a dilute suspensions of axisymmetric Brownian particles, Int. J. Multiph. Flow 1 (1974) 195–341.
[101] E.J. Hinch, L.G. Leal, The effect of Brownian motion on the rheological properties of a suspension of non-spherical particles, J. Fluid Mech. 52 (1972) 683–712.
[102] C.J.S. Petrie, The rheology of fibre suspensions, J. Non-Newton. Fluid Mech. 87 (1999) 369–402.
[103] H. Brenner, D.W. Condiff, Transport mechanics in systems of orientable particles. 4. Convective transport, J. Colloid Interface Sci. 47 (1974) 199–264.
[104] S.B. Chen, D.L. Koch, Rheology of dilute suspensions of charged fibers, Phys. Fluids 8 (1996) 2792–2807.
[105] A. Sokolov, I.S. Aranson, Reduction of viscosity in suspension of swimming bacteria, Phys. Rev. Lett. 103 (2009) 148101.
[106] S. Rafaï, L. Jibuti, P. Peyla, Effective viscosity of microswimmer suspensions, Phys. Rev. Lett. 104 (2010) 098102.
[107] J. Gachelin, G. Miño, H. Berthet, A. Lindner, A. Rousselet, E. Clément, Non-Newtonian viscosity of *E. coli* suspensions, submitted for publication.
[108] B.M. Haines, I.S. Aranson, L. Berlyand, D.A. Karpeev, Effective viscosity of bacterial suspensions: A three-dimensional PDE model with stochastic torque, Commun. Pure Anal. 11 (2012) 19–46.
[109] D. Marenduzzo, E. Orlandini, J.M. Yeomans, Hydrodynamics and rheology of active liquid crystals: A numerical investigation, Phys. Rev. Lett. 98 (2007) 118102.
[110] M.E. Cates, S.M. Fielding, D. Marenduzzo, E. Orlandini, J.M. Yeomans, Shearing active gels close to the isotropic-nematic transition, Phys. Rev. Lett. 101 (2008) 068102.

[111] Z. Cui, Weakly sheared active suspensions: Hydrodynamics, stability, and rheology, Phys. Rev. E 83 (2011) 031911.
[112] L. Giomi, T.B. Liverpool, M.C. Marchetti, Sheared active fluids: Thickening, thinning, and vanishing viscosity, Phys. Rev. E 81 (2010) 051908.
[113] S. Heidenreich, S. Hess, S.H.L. Klapp, Nonlinear rheology of active particle suspensions: Insights from an analytical approach, Phys. Rev. E 83 (2011) 011907.
[114] L.H. Cisneros, J.O. Kessler, S. Ganguly, R.E. Goldstein, Dynamics of swimming bacteria: Transition to directional order at high concentration, Phys. Rev. E 83 (2011) 061907.
[115] N.C. Darnton, L. Turner, S. Rojevsky, H.C. Berg, Dynamics of bacterial swarming, Biophys. J. 98 (2010) 2082–2090.
[116] H.P. Zhang, A. Be'er, E.-L. Florin, H.L. Swinney, Collective motion and density fluctuations in bacterial colonies, Proc. Natl. Acad. Sci. USA 107 (2010) 13626–13630.
[117] X. Chen, X. Dong, A. Be'er, H.L. Swinney, H.P. Zhang, Scale-invariant correlations in dynamics bacterial clusters, Phys. Rev. Lett. 108 (2012) 148101.
[118] P.G. de Gennes, J. Prost, The Physics of Liquid Crystals, Clarendon Press, Oxford, 1993.
[119] P.G. de Gennes, Phenomenology of short-range-order effects in the isotropic phase of nematic materials, Phys. Lett. A 30 (1969) 454–455.
[120] T.B. Liverpool, M.C. Marchetti, Hydrodynamics and rheology of active polar filaments, in: P. Lenz (Ed.), Cell Motility, Springer, 2008, pp. 177–206.
[121] L. Giomi, M.C. Marchetti, T.B. Liverpool, Complex spontaneous flows and concentration banding in active polar films, Phys. Rev. Lett. 101 (2008) 198101.
[122] I.S. Aranson, A. Sokolov, J.O. Kessler, R.E. Goldstein, Model for dynamical coherence in thin films of self-propelled microorganisms, Phys. Rev. E 75 (2007) 040901.
[123] W. Maier, A. Saupe, Eine einfache molekulare Theorie des nematischen kristallinflüssigen Zustandes, Z. Naturforsch. 13 (1958) 564–566.
[124] D.J. Jeffrey, J.F. Morris, J.F. Brady, The pressure moments for two spheres in a low-Reynolds-number flow, Phys. Fluids A 5 (1993) 2317–2325.
[125] P.R. Nott, J.F. Brady, Pressure-driven flow of suspensions: Simulation and theory, J. Fluid Mech. 275 (1994) 157–199.
[126] P.R. Nott, E. Guazzelli, O. Pouliquen, The suspension balance model revisited, Phys. Fluids 23 (2011) 043304.
[127] D.A. Brown, H.C. Berg, Temporal stimulation of chemotaxis in *Escherichia coli*, Proc. Natl. Acad. Sci. USA 71 (1974) 1388–1392.
[128] R.N. Bearon, T.J. Pedley, Modelling run-and-tumble chemotaxis in a shear flow, Bull. Math. Biol. 62 (2000) 775–791.
[129] G. Subramanian, D.L. Koch, S.R. Fitzgibbon, The stability of a homogeneous suspension of chemotactic bacteria, Phys. Fluids 23 (2011) 041901.
[130] T.V. Kasyap, D.L. Koch, Chemotaxis driven instability of a confined bacterial suspension, Phys. Rev. Lett. 108 (2012) 038101.
[131] E. Lushi, R.E. Goldstein, M.J. Shelley, Collective chemotactic dynamics in the presence of self-generated fluid flows, Phys. Rev. E 86 (2012) 040902.
[132] E.O. Budrene, H.C. Berg, Complex patterns formed by motile cells of *Escherichia coli*, Nature 349 (1991) 630–633.
[133] B.L. Bassler, Small talk: Cell-to-cell communication in bacteria, Cell 109 (2002) 421–424.
[134] S. Park, P.M. Wolanin, E.A. Yuzbashyan, P. Silberzan, J.B. Stock, R.H. Austin, Motion to form a quorum, Science 301 (2003) 188.
[135] E.F. Keller, L.A. Segel, Model for chemotaxis, J. Theor. Biol. 30 (1971) 225–234.
[136] M.P. Brenner, L. Levitov, E. Budrene, Physical mechanisms for chemotactic pattern formation by bacteria, Biophys. J. 74 (1998) 1677–1693.
[137] W. Alt, Biased random walk models for chemotaxis and related diffusion approximations, J. Math. Biol. 9 (1980) 147–177.
[138] K.C. Chen, R.M. Ford, P.T. Cummings, Cell balance equation for chemotactic bacteria with a biphasic tumbling frequency, J. Math. Biol. 47 (2003) 518–546.
[139] E. Lushi, R.E. Goldstein, M.J. Shelley, Auto-chemotactic active suspensions: Modeling, analysis and simulations, submitted for publication.
[140] J.G. Gibbs, S. Kothari, D. Saintillan, Y.-P. Zhao, Geometrically designing the kinematic behavior of catalytic nanomotors, Nano Lett. 11 (2011) 2543–2550.
[141] D. Takagi, A.B. Braunschweig, J. Zhang, M.J. Shelley, Dispersion of self-propelled rods undergoing fluctuation-driven flips, Phys. Rev. Lett. 110 (2013) 038301.
[142] G.H. Koenderink, Z. Dogic, F. Nakamura, P.M. Bendix, F.C. MacKintosh, J.H. Hartwig, T.P. Stossel, D.A. Weitz, An active biopolymer network controlled by bimolecular motors, Proc. Natl. Acad. Sci. USA 106 (2009) 15192–15197.
[143] S. Ramaswamy, The mechanics and statistics of active matter, Annu. Rev. Condens. Matter Phys. 1 (2010) 323–345.
[144] M.C. Marchetti, J.F. Joanny, S. Ramaswamy, T.B. Liverpool, J. Prost, M. Rao, R. Aditi Simha, Soft active matter, Rev. Mod. Phys. (2011), submitted for publication.
[145] N. Darnton, L. Turner, K. Breuer, H.C. Berg, Moving fluid with bacterial carpets, Biophys. J. 86 (2004) 1863–1870.
[146] A. Sokolov, M.M. Apodaca, B.A. Grzybowski, I.S. Aranson, Swimming bacteria power microscopic gears, Proc. Natl. Acad. Sci. USA 107 (2010) 969–974.
[147] R. Di Leonardo, L. Angelani, D. Dell'Arciprete, G. Ruocco, V. Iebba, S. Schippa, M.P. Conte, F. Mecarini, F. De Angelis, E. Di Fabrizio, Bacterial ratchet motors, Proc. Natl. Acad. Sci. USA 107 (2010) 9541–9545.
[148] E.B. Steager, M.S. Sakar, D.H. Kim, V. Kumar, G.J. Pappas, M.J. Kim, Electrokinetic and optical control of bacterial microrobots, J. Micromech. Microeng. 21 (2011) 035001.